AD_____

Award Number: W81XWH-08-1-0289

TITLE: Characterizing the Relationship Between Blast Exposure and Mild TBI with Dynamic Modeling and Testing in a New Mouse Model

PRINCIPAL INVESTIGATOR: Candace L. Floyd, Ph.D.
W. Steve Shepard, Jr., Ph.D.

CONTRACTING ORGANIZATION: The University of Alabama at Birmingham
Birmingham, AL 35249

REPORT DATE: July 2011

TYPE OF REPORT: Annual

PREPARED FOR: U.S. Army Medical Research and Materiel Command
Fort Detrick, Maryland 21702-5012

REPORT DOCUMENTATION PAGE

Form Approved
OMB No. 0704-0188

1. REPORT DATE	2. REPORT TYPE	3. DATES COVERED
July 2011	Annual	1 July 2010 – 30 June 2011

4. TITLE AND SUBTITLE

Characterizing the Relationship Between Blast Exposure and Mild TBI with Dynamic Modeling and Testing in a New Mouse Model

5a. CONTRACT NUMBER

5b. GRANT NUMBER
W81XWH-08-1-0289

5c. PROGRAM ELEMENT NUMBER

6. AUTHOR(S)

Candace L. Floyd, Ph.D.
W. Steve Shepard, Jr., Ph.D.

E-Mail: clfloyd@uab.edu

5d. PROJECT NUMBER

5e. TASK NUMBER

5f. WORK UNIT NUMBER

7. PERFORMING ORGANIZATION NAME(S) AND ADDRESS(ES)

The University of Alabama at Birmingham
Birmingham, AL 35249

8. PERFORMING ORGANIZATION REPORT NUMBER

9. SPONSORING / MONITORING AGENCY NAME(S) AND ADDRESS(ES)
U.S. Army Medical Research and Materiel Command
Fort Detrick, Maryland 21702-5012

10. SPONSOR/MONITOR'S ACRONYM(S)

11. SPONSOR/MONITOR'S REPORT NUMBER(S)

12. DISTRIBUTION / AVAILABILITY STATEMENT
Approved for Public Release; Distribution Unlimited

13. SUPPLEMENTARY NOTES

14. ABSTRACT

The purpose of this research is to determine through analytical modeling and animal-based experiments the blast-level threshold for mild traumatic brain injury in humans. We have cataloged brain material properties and determined microtubule geometry and response to mechanical loading. Basic axon geometry has been determined for a finite element (FE) model and modified geometry has also been developed. Blast pressure profiles for small IED and other blast scenarios have been determined from literature reviews. Preliminary models and test fixtures have been constructed. In a tandem effort, laboratory-based animal experiments are being conducted to determine the effects of impact-induced or blast-induced mTBI on loss of consciousness, vestibular motor ability, learning and memory, anxiety, depression, insomnia, and compulsive behaviors. Also, evaluation as to the brain regions with diffuse axonal injury or myelin damage is being conducted. In summary, FE modeling of axon geometry and related blast profiles for models are being completed and will be related to laboratory-based experimentation.

15. SUBJECT TERMS
Mild traumatic brain injury, finite element analysis, axonal geometry, blast injury

16. SECURITY CLASSIFICATION OF:			17. LIMITATION OF ABSTRACT	18. NUMBER OF PAGES	19a. NAME OF RESPONSIBLE PERSON
a. REPORT	b. ABSTRACT	c. THIS PAGE			USAMRMC
U	U	U	UU	43	19b. TELEPHONE NUMBER *(include area code)*

Table of Contents

Introduction:

The purpose of this research is to determine through analytical modeling and animal-based experiments the blast-level threshold for mild traumatic brain injury in humans. Mild traumatic brain injury (mTBI) is known to occur in humans subjected to explosive blast levels that do not induce external or measurable internal injuries. As a result, it is not known until a later date the mTBI has been experienced. Through analytical modeling in this research, the blast-induced internal strain and rates of strain in the human brain are going to be determined. Determining these levels will be accomplished by simulating the structure of the brain subjected to blast levels found in the literature. Then, corresponding mouse brain models will be developed in order to determine the analogous response parameters in those scaled brains. In a tandem effort, laboratory-based animal experiments are being conducted to determine the blast-pressures and impact-acceleration parameters that induce mTBI in mice. Once the impact-acceleration and blast levels that cause mTBI in animals are understood, it will be possible to use the animal-based analytical models to determine the corresponding brain response parameters. These brain response parameters will then be scaled to the human brain analytical modeling so that the blast pressures that generate these response rates can be determined.

Body:

This section provides an overview of the work and accomplishments. The approved tasks from the Statement of Work are provided in *italics*. Below those statements, the corresponding progress from June 2010-June 2011 is detailed. Statements are also made with regard to work in progress or that has yet to be done.

Statement of Work:

To test the hypotheses, and numerical simulations and animal-based experiments will be conducted. The specific aims, as described in this proposal, will be achieved by collaborative research between the Department of Physical Medicine and Rehabilitation at The University of Alabama at Birmingham (UAB) and the Department of Mechanical Engineering at The University of Alabama (UA). UAB and UA are only about 50 miles apart, which will facilitate convenient and frequent meetings between the two groups. The specific tasks to reach the research aims include:

Task 1: Initialization of project and organization of collaborative team

This task has been completed. Frequent email and phone correspondence occurs between the collaborative teams with quarterly group meetings held to transfer ideas and discuss progress.

Task 2: Simulation of full-scale blast scenarios using a dynamic model

In recent years, there has been a growing wealth of research related to brain injury modeling. The goal of these works has been to accurately model the brain in order to evaluate and understand injuries that occur under different loading scenarios. One of the primary brain mechanical modeling approaches has been through the use of whole-head models, like the Wayne State Brain Injury Model. These whole-head models are complex and encompass many of the structural components within the head (6). In these types of models, different mechanical

loading scenarios, such as accelerations and impulses, are imposed on the head and various response parameters, like strains, stresses, and strain-rates, are evaluated. The ability to solve this type of finite element model relies heavily on the fact that the material properties of the brain are treated as homogenous. It is clearly not feasible to model the microstructures that makeup materials such as the brain white matter. As a result of the need to use homogeneous material properties, the results of these simulations can be inconclusive from the perspective of understanding the underlying injury mechanisms. The inability to understand the underlying mechanisms that produce injury has hindered the determination of specific brain injury thresholds, such as given accelerations or blast pressures.

Studies have shown that the more severe consequences of mTBI occur at a microscopic level. The axon, which is responsible for the transmission of information throughout the brain, is comprised of many microscopic components. Of these components, axons get most of their structural support characteristics from microtubules and neurofilaments (7). Microtubules, hollow nanoscale components, provide important structural support and transport pathways that aide in the axons ability to function (8). The impact of mechanical loading on these microscopic structures has not been assessed in detail due to the need to use homogeneous properties in the whole-head models described earlier. Again, it is not practical from the computational perspective to model these structures on the nanometer scale in these whole-head models. While there have been some studies involving measurement of the global properties of groups of these microstructures, little research aimed at examining their mechanical response in detail as a single structure has been conducted. Two notable studies are the works of de Pablo *et. al* (11) and Schaap *et. al.* (12), which are discussed in more detail below. Since the health of axons is known to depend on these microstructures, the goal of the research described here involves examination of brain injury modeling, but from a more microscopic perspective. To that end, the work cited above was used as a starting place in order to examine mTBI via modeling, but from the perspective of microtubule (MT) failure. Note that this work is a continuation of the work described in last year's annual report. Furthermore, the direction of the work, as described in last year's report, has been enhanced with the goal of obtaining the more fundamental understanding of brain injury, as opposed to following the originally planned path and potentially missing those fundamental mechanisms.

Of the rod-like structures mentioned above, microtubules, MTs, are the most rigid (9). In works mentioned above, the elastic properties of MTs were measured using atomic force microscopy (AFM) by subjecting a single MT sample to radial loads and observing the MT's reaction (11). From those experiments, it was observed that when a radial scanning load exceeding 300 pN was applied to a microtubule, as denoted by F_{max} and illustrated in **Figure 1**, irreversible damage occurred. Yet, when a scanning load less than 300 pN was applied, the MT always returned to its original shape. This force, albeit approximate, provides the starting point for this research project to evaluate the failure mechanisms within this brain microstructure via numerical modeling.

In order to perform such a study to determine the response thresholds associated with failure, an appropriate geometric representation of the MT is needed. In recent work by Schaap *et. al*. (12), equivalent elastic mechanical properties for MTs were determined. From that work, an effective geometric representation was determined by using finite element methods. This more simplified geometry is used here, where the microtubule is to be modeled as a simple hollow tube with an outer diameter of 19.88 nm and an inner diameter of 16.8 nm. By using all-

atom simulation systems and continuum elastic modeling, Sept and MacKintosh were able to calculate a Young's modulus of 2.2 GPa for a MT (10). By utilizing the results of the works mentioned above, the specific goal of the research described here is to correlate loading in the previously conducted AFM experiments (11, 12), as illustrated in **Figure 2**, via modeling in order to determine an equivalent response characteristic associated with MT failure. The ultimate benefit of this research is to provide specific MT failure characteristics and enable those modelers using a whole-head approach with the ability to better predict mTBI through the continued use of homogeneous material properties.

As noted above, this portion of the research involves a study in which previously conducted AFM experiments (11, 12) involving microtubule mechanical failure are being examined using finite element methods. One important issue that must be addressed involves a reasonable description of the complex loading provided by the AFM tip as well as the boundary conditions. Because of the complex nature of the AFM loading, several different models are utilized to help gain a better understanding of the important characteristics of that loading. Note that this correlation study with the AFM loading only examines the static considerations. Current studies, described below as well as for another task, involve extending the stresses obtained in that static model to dynamic studies, which will provide a better understand how wave motion impacts the MT structure. Not only will the *in vitro* condition for the AFM be modeled, but the *in vivo* conditions that a MT would experience are also examined. The AFM loading study involves further complications in attempting to correlate an AFM failure load with an analogous distributed load experienced *in vivo*. Besides the type of loading, there are several other important considerations that must also be considered in the *in vivo* portion of the study. For example, the impact of nearby MTs on the response characteristics were examined. Because axonal MTs are collinear, the effect of other nearby structures on the resulting response can be an important characteristic. The following reviews the structure of the MT along with other topics relevant to the finite element models used in the simulations. As will be seen, each of these models differs primarily in the manner in which the loading is applied. Once those topics are addressed, results from the simulations are provided along with some general discussion of the observations made to date.

FEA MODELS

Several Finite Element models were developed and are being considered. These models include: the point load (PL), rigid press (RP), atomic force microscopy single element (AFMSE), atomic force microscopy full (AFMF), and composite single element (CSE) models. All of these models are considered *in vitro* except for the CSE model, which attempts to represent the MT *in vivo*. In these models, 20-node brick elements are used to mesh the various materials. All material properties are assumed to be linear isotropic. More complicated material properties, such as nonlinear, will be considered once the methodology for correlating AFM loading with the transient blasé wave-loading studies has been conducted and confirmed. Although not discussed or shown, convergence studies for these models have been performed to ensure the accuracy of the results (some figures have yet to be updated accordingly).

POINT LOAD (PL) MODEL

In the PL model shown in **Figure 2a**, a microtubule of a finite length of 100 nm is subjected to a point loading of 300 pN at the top while a pinned constraint is applied to a line of nodes along

the length of the bottom of the MT. This model represents the AFM experiments with the assumption that the AFM produces a concentrated point load.

RIGID PRESS (RP) MODEL

The rigid press (RP) model illustrated in **Figure 3** allows for a potentially more accurate description of the loading mechanics that arise in the microtubule. The RP model allows for an understanding of the y-direction stresses that arise in the PL model. The mechanics in the RP model are based on the fact that the radius of the AFM tip, 20 nm, is relatively large compared to the radius of the microtubule, 9.94 nm. This tube is loaded on the upper and lower surfaces by two steel plates. To represent an infinite MT, a 2 nm long model is constructed with symmetric boundary conditions on each xy face of the model in the z-direction. A load based on the upper area of the top plate is initially used. This load, initially 6 MPa, is derived by adjusting the pressure magnitude on the top plate until the stresses in the y-direction match that of the PL model, which ends up being 0.238 MPa. Furthermore, the base of the bottom plate is rigidly constrained in all directions to further represent the conditions of the AFM experiments. By using this approach, the impact of the tip loading of stresses in the other directions can more readily be assessed.

ATOMIC FORCE MICROSCOPY SINGLE ELEMENT (AFMSE) MODEL

Even with the understanding provided by the above models, another model was created to better simulate the AFM tip loading geometry. To accomplish this, the upper plate in the PB model is refined to be more geometrically similar to an AFM tip, as shown in **Figure 4**. Because of the size of the AFM tip in the relation to the MT size, as noted above, localized loading of this nature may be similar to that produced by an infinitely long tip. As a result, a model that represents an infinitely long AFM tip with the same radius was examined through the Atomic Force Microscopy Single Element (AFMSE) model. This model consists of three component cross sections: the AFM tip, the MT, and a rigid base, all of which are 2 nm wide. The AFM tip with a radius of 20 nm is loaded with a distributed loading on the top surface. The base of the bottom steel plate is constrained rigidly in all directions, again to replicate the AFM experiments. It should be noted that the axial faces have symmetric boundary conditions to represent the aforementioned infinitely long MT and tip.

ATOMIC FORCE MICROSCOPY FULL (AFMF) MODEL

Further motivation to understand the scale of the AFM tip in the previous experiment, a model that includes a finite AFM tip geometry was produced. This model is called the AFMF model as illustrated in **Figure 5.** In this model, the AFM tip is treated as a hemisphere in contact with a finite length hollow tube. The tube is resting on a steel plate, which is pinned in all directions. As in the previous model, a distributed load is applied to the top surface of the AFM tip. In the AFMF model, contact elements are used to control the interaction between the AFM tip and the microtubule.

One might at this point question the need for the above-mentioned models when the AFMF appears to better represent the actual geometry of the AFM experiment. By utilizing these different approaches, it is hoped that the important characteristics of the failure mechanics can be more readily identified and then correlated with the semi-infinite two-dimensional wave

propagation models currently being developed and examined. These characteristics will be noted in the results section below.

COMPOSITE SINGLE ELEMENT (CSE) MODEL

All of the models described thus far consider AFM loading of the microtubule from an *in vitro* perspective. Again, this is done to help correlate the important MT response characteristics with the failure observed in AFM experiments. In order to correlate the important response results to MT failure associated with mTBI, it is necessary to account for the effects of the cytoplasm that is known to surround and fill the MT in the axon. The Composite Single Element (CSE) model was created to examine this configuration. This model is considered to be *in vivo* because it is representing an infinite tube suspended in cytoplasm, as illustrated in **Figure 6.** Here the MT is sliced vertically in half length-wise to impose symmetry along that axis. The base of the model has a pinned constraint in all directions, and the CSE model has symmetry imposed in the x and z directions.

In this model, the impact that neighboring MTs have on the loading and stress distribution has been easily examined by adjusting the distance between the microtubule and the cytoplasm boundary where symmetry is imposed. At this symmetry face, a mirror of the MT is provided such that an array of equally spaced MTs is actually being considered. The impact of the nearby MTs may impact the resulting stresses in the MT and provide a lower or higher threshold for mTBI from a failure of this component. By varying the dimensions of the geometry in this relatively simple single-element width model, the impact of nearby MTs can be studied with greater ease. Furthermore, the impact of nearby boundaries can be examined by adjusting the distance of the MT from the lower boundary, where a rigid boundary condition is imposed. This study is useful in examining the impact of nearby rigid structures within the brain, such as bones or other structures, on the MT response.

SIMULATION RESULTS

As noted earlier, a model was first created to represent the AFM experiments with the assumption that the AFM produces a concentrated point load. From the analysis of the PL model, a high stress concentration around the point load is seen in **Figure 2**. Neglecting those stress concentrations, the next extreme y-stresses are located as expected midway on the inside of the tube. The values for these stresses are 22.47 MPa and -28.18 MPa respectively. Note that due to the presence of a bending stress and a superimposed axial stress, these extreme stress values are not symmetric. As with typical convention, a positive value denotes a tensional stress while a negative stress denotes compression. Observing that the PL model has a stress concentration around the location of the load, the Rigid Press (RP) model with loading that creates the same y-direction stresses was examined. The RP serves as an aide in beginning to understand of the loading mechanics that were present in the AFM experiments. To generate the same y-direction stresses as the PL model, the pressure is adjusted until the RP model gives similar stress results. It can be seen that the extreme y-direction stresses occur at the same location of the MT as in the PL model as seen in **Figure 3** and result from a 0.238 MPa applied pressure. The values in the y-direction that match the RP model are 22.26 MPa and -28.40 MPa respectively. Comparing the average between the max and min PL y-stresses to those of the RP model, it can be seen that they both share an average of 25.3 MPa. Also, in comparing the z-direction stresses (not shown) located at the same nodes as the extreme y-direction stress, there

is an approximately 400 percent increase from the PL model to the RP model. However these z-direction stresses that are being compared are only 6 to 30 percent of the y-direction stresses. From the RP model, it can be seen that the assumption that the extreme y-direction stresses are important characteristics in determining failure criterion for microtubules and it gives a starting applied load for the models that require a pressure.

The AFMSE model is originally analyzed with a load of 3.75 MPa, which produces a load of 300 pN on the upper surface of the AFM tip. This load produces extreme y-direction stresses that occur at the same location of the previous models as illustrated in **Figure 4**. The values of the max and min are very large when compared to those of the PL and RP models. This is, however, expected due to the fact that symmetry is being imposed and the total load on the MT will be significantly larger than a real MT would experience from an AFM tip. The point of this model, though, is to move towards determining what distributed loads impact the MT in the same manner. As a result, the 0.238 MPa pressure is scaled based on the relative width of the AFM tip in comparison to the plate in the RP model. This scaled pressure, 0.148 MPa, produces extreme stresses of -22.84 MPa and 18.57 MPa. The stresses associated with this new pressure loading can be seen in **Figure 4**. When compared to the results of the PL and RP models, the y-stresses found in the AFMSE model are approximately 18 percent smaller. Also, the z-direction stressed at the same nodes show a similar 18 percent decrease while the x-direction stresses incur a 200 percent increase.

To further examine the effect of the tip radius on the microtubule response, the AFMF model enables study of a finite length tube in contact with a more true depiction of the AFM tip. With an area based load of 0.238 MPa applied to the top surface of the tip, the maximum y-direction stress occurs at the same location as all previous models, which is 20.20 MPa as seen in **Figure 5.** Unlike some of the previous models, a stress concentration occurs at the location where the tip contacts with the microtubule, producing a minimum y-direction stress at this location. If this concentration is ignored, the next minimum occurs in the same place as all other models and has a value of -25.89 MPa. Taking the average of the extreme values of the AFMF model and comparing it to the average values found in the PL, RP, and AFMSE models, the AFMF model's average is approximately 9 percent lower. This reduction could be a direct result of the shape of the AFM tip in relation to the MT. The above models show that the resulting stresses in the y-direction were a likely candidate for structural failure due to bending stresses and axial loading components in the vertical direction that occur on the sides of the MT. Furthermore, with equivalent loading these models all share the approximate y-direction stress.

The results described thus far represent the loading mechanics of microtubules when the configuration is representative of *in vitro* conditions. In order to extend the insight gained above and to account for an *in vivo* scenario, the Composite Single Element (CSE) model was used. A 0.12 MPa load, an arbitrary value, was initially applied to the top surface of the cytoplasm. In order to quantify the impact that neighboring MTs on the resulting MT stress distribution, the distance between the boundary and the MT structure was adjusted. **Figure 7** shows the impact of the horizontal spacing of microtubules on the maximum Von Mises Stress in the microtubule. Note that in this simulation, the lower boundary is sufficiently far away to eliminate its impact on the MT stress (see discussion below). As can be seen in the figure, a nearby MT does not begin to impact the stresses until the MTs are closer than about 80 nanometers. As the distance between MTs decreases, the maximum von Mises stress in the MT increases. This type of increase in stress is because more of the loading is imposed on the microtubules and when the

spacing greater than the 80 nm, the cytoplasm is bearing most of the load. It has been found that motor proteins that interconnect microtubules provide a range in spacing of approximately 10 nm to 20 nm between connected MTs (13 ,14). As a result, this simulation shows that the stresses seen in MTs in the axon will be slightly higher due to nearby MTs.

To examine the impact of a nearby rigid boundary, **Figure 8** shows the influence of the vertical spacing of MTs relative to the lower rigid boundary condition on the maximum von Mises stress. It can be seen in the figure that the rigid boundary's location in relation to the microtubule has a small impact on the stress with the MT. The associated increase in the overall von Mises stress that occurs as the rigid boundary distance decreases from 60 nm to 2.5 nm is only about 6 percent. From this, it can be seen that the rigid boundary location in relation to the MT has little effect on the von Mises stresses of the MT, except when the MT is very close to the rigid structural boundary.

In addition to evaluating the impact of nearby microtubules and rigid boundaries, the CSE is also used to gauge the y-direction stresses that arise as a result of pressure loading. By using the results of the spacing analysis, a model utilizing boundary distances found above that do not affect the stresses was generated. This model has a horizontal boundary set at 80 nm and a bottom rigid boundary at 15 nm. In this model, seen in Figure (2.6b), a load is applied until the y-direction stresses match those of the PL, RP, AFMSE, and AFMF models. In this case, a pressure of 3.75 MPa is needed, which results in a minimum y-stress of -28.12 MPa. However, in the same model (CSE) the maximum y-stress is 0.014 MPa, which in comparison is much smaller than the resulting maximums that occurred in all previous models. This decrease in the maximum y-stress results from the cytoplasm sharing the applied load and changing the stress characteristics in the MT. It can be seen that the cytoplasm plays an important role in the mechanical loading characteristics of microtubules. On the other hand, the resulting negative y-direction bending stress that is present in the interior of the MT could play a significant role in the determination of failure criterion of MTs. However, in the CSE model the axial loading components in the vertical direction outweigh the bending components.

In order to better understand the loading effects and compare the static and dynamic loading conditions described below, the models are being transitioned to cylindrical coordinates. By using cylindrical coordinates, the stress values around the MT periphery can be compared more effectively in terms of tangential and radial stresses, along with the axial stresses already examined. These changes are currently being made to the model and the results will be described in the final report.

NOTABLE OUTCOMES

In previous modeling studies, brain injury has been evaluated from a macroscopic point of view and axonal injuries have been examined through the computation of stresses, strains, and strain rates. However, the approach taken in those studies has been with assumed homogeneous material properties for the white and grey matter. The research presented here numerically studies brain injury from a microscopic perspective, focusing on the mechanical response characteristics of microtubules. Using loads found by other researchers that result in permanent microtubule damage during atomic force microscopy experiments, an analysis using finite element models is being conducted in this research. These models include the Point Load (PL), Rigid Press (RP), Atomic Force Microscopy Single Element (AFMSE), Atomic Force

Microscopy Full (AFMF), and the Composite Single Element (CSE). The PL model examines the assumption of a point load and provided y-direction stresses to be used for comparison purposes. The RP model is used to match the results of the PL model and required a distributed load of 0.238 MPa to do that. In the AFMSE model, this 0.238 MPa load was scaled based on the relative width, which gave y stresses that were 18 percent lower than the RP model. The AFMF model captures a more accurate depiction of the AFM experiments and gives insight to the relation of the AFM tip and the extreme stress magnitudes.

The CSE model was initially used to shed insight on the impact of nearby microtubules. That study showed that stresses begin to increase as the distance between MTs decreases below 80 nm. Furthermore, since it is known that the relative MT spacing provided by the motor proteins is approximately 10 to 20 nm, the expected stresses within the MT will be higher when a motor protein has joined to MTs. Except for very close rigid boundaries opposite the loading direction, the impact of these nearby rigid boundaries was shown not to be so important. Future work will focus on setting failure thresholds and evaluating the results of models that include dynamic wave propagation like that experienced during a blast-loading event. Some preliminary results in this area are discussed in another task below.

Task 3: Characterize fundamental parameters for dynamic mouse model of mTBI using an impact acceleration model

In the previous work summarized in the last report, we evaluated the duration of transient unconsciousness, post-impact vestibular motor performance, post-impact learning and memory and post-impact anxiety. To complete this task, in this year we evaluated the effect of impact-acceleration mTBI on home-cage behaviors to assess sleep/insomnia, fatigue/depression, and other mood/state changes. Specifically we examine depression/despair using the forced swim task, consumption of food and water in the bioactivity chamber, grooming duration as an indicator of compulsive behavior, and duration of immobility in the light and dark cycle as an evaluation of sleep/insomina. For these experiments, mice were individually housed and evaluated using the LABORAS monitoring system (Metris, Inc.). The LABORAS is a non-invasive behavioral monitoring system that automatically recognizes and quantifies several normal and abnormal behaviors of mice (**Figure 9)**. For these experiments, mice were placed in the home cage in the LABORAS monitoring system for 5 days to obtain baseline behaviors. Then mice were randomly assigned to either sham, blast-induced, or impact-induced mTBI groups. One hour after the induction of the brain injury (or sham), mice were returned to the LABORAS home-cage and monitored for a subsequent 6 days post-TBI. Although the data analysis from the vast set of data obtained from the LABORAS system are currently being regerously evaluated, preliminary data suggest the impact- or blast-induced mTBI induces differences in home cage behaviors. For example, resting or immobility is defined as a period when movement is absent while the animal is in a sitting or lying position. The results of this experiment are combined with the results obtained in *task 7*, and as such are presented with discussion of that task, below.

Task 4: Study loading on the brain via simulation

As described for Task 2, the objective in studying the onset of brain injury involves a detailed numerical simulation of microstructures within the brain. That section provides a

detailed explanation of the approach taken (as also described in last year's report) and some of the simulation results of interest. As part of the effort, the simulation results obtained in the static modeling must be correlated to dynamics waves propagating through the brain. This is necessary so that the dynamic effects of loading, including inertial and elastic effects, on these microstructures can be understood. Then, it will be possible to obtain actual blast pressure loading levels that are believed to produce actual microstructure damage. Furthermore, the impact of various loading directions and pulse scenarios can be examined to determine how such parameters impact the stress response of these microstructures. While this portion of the study is ongoing, some preliminary results are available and are described here.

TRANSIENT WAVE LOADING IN MICROTUBULES LEADING TO FAILURE

The infinite MT filled with cytoplasm and finite length MT with cytoplasm have been analyzed to reveal maximum stress values which will yield the MT cylinder structure when subjected to a pressure load impacted with a time period of 3.04×10^{-9} s. A stress wave propagation caused by this pressure load will travel through MT and cytoplasm assembly. The material properties in Young's modulus of microtubule are 2.2 GPa, MT density at 1470 kgm^3 and Poisson ratio 0.3. For the surrounding cytoplasm medium, Young's modulus is 1kPa, density is 1040 kgm^{-3} and Poisson ratio is 0.499. As expected, the maximum stress values in the microtubules occur when the wave loads passes through the MT strucutre. In these FEM models, illustrated in **Figures 10 and 11**, all elements are solids. These models were excited by a pressure load of 11.3 MPa initially at the top surface close to the microtubule structure and produce stress waves propagating along the y direction of the model. The applied pressure is refined until the minimum tangential stress (cylindrical coordinates) within the MT reaches -84.1 MPa, where the pressure required to attain that stress is 1.25 MPa. The time at which this occurs is 1.4×10^{-09}s. Sample results when the wave has just passed the MT are shown in Figure (4.1). As noted above, one important aspect involves shifting the simulation into cylindrical coordinates. This is being done so that the results from static model, along with the single parameter stresses like von Mises and Princpal, can be compared with those obtained in the dynamic wave propagation model. The impact of nearby structures will also be examined, just as for the static results described in Task 2. These studies are ongoing and the results will be reported next year, along with the blast pressures believed to produce the onset of mild traumatic brain injury. Preliminary results showing a comparison on the static stress results and the dynamic (blast loading) transient results for the microtubule in the cytoplasm model are shown in **Figure 11**. Note that since the models are being transitioned to the cylindrical coordinates, results will be provided in an upcoming paper and in next year's final report.

Task 5: Develop a dynamic mouse model of blast injury

As discussed above as well as in last year's annual report, it was determined during earlier portions of the research that a more effective modeling approach would involve study of brain injury from the microscopic perspective. By utilizing this approach, which involves the development of additional models, it is not as essential to develop a full model consisting of the animal's anatomy. As such, once the loading mechanisms for the animal are understood from experiments and correlated with the model efforts described in Task 2, it will be possible to quickly extrapolate those results to human blast pressure levels. By gaining a more fundamental

understanding of the loading and damage onset of microstructures, through modeling, it will be possible to examine various loading scenarios and the resulting stresses and strains. Some of the current results are described above as related to the microtubule modeling. As a result, those results are not repeated here. Instead, refer to the results provided under Task 2 and in Task 4 as well as in the Appendix. Some of the curve fitting performed on actual blast pressure data is described in Task 8. We will continue with this task in the upcoming year.

Task 6: Development of test system and fixture configurations

Aspects of the test system and fixture configurations were evaluated and as such test fixture evaluation was divided into 5 components: the blast source, the shock tube/blast housing, the specimen restraint, the transducer, and the rebounding wave absorber. For each of these sections, multiple options were considered and evaluated through certain criteria, which are discussed below. As described last year, the preliminary concept for the blast source was to use a modified Hilti Tool to detonate .22 caliber charges as the blast source. Alternative approaches we evaluated were the use of a starter pistol to detonate 0.22 caliber blank charges and a paintball gun to detonate a compressed air wave. As for the shock tube/blast housing, options to be evaluated were three types of piping: PVC, aluminum, and steel. The main advantage to using piping material is that the dimensions (length and diameter) could be easily and systematically varied and that the reflections would be somewhat uniform and reproducible. The specimen restraint will be custom built based upon the design parameters to build a rectangular box that will house the mouse's body and have a small hole that will only expose the head. With this design our theory that the pressure wave will predominately affect the brain as the exposure to the body cavity will be greatly reduced. The custom restraint will also be mounted onto a platform which can be easily repositioned such that the specimen can be positioned in various locations within the blast tube or at a specified distance from the tube so that different peak pressure can be achieved at these various distances. As for the transducers we have chosen two pressure transducers and one rupture membrane for our options. The membranes rupture at different known pressure. The two transducers read out pressures and post-processing would be required to determine the characteristics of the wave to which the mouse's head and/or brain are exposed. The rebound wave absorber will also be custom constructed such that a cube frame will be surrounded with a shock/ sound wave absorption foam.

Criteria for the preliminary ranking and evaluation possible options for each subsystem will include cost, user-friendliness, reproducibility, safety (both operator and specimen), and construction/maintenance. Cost will be an important factor critical to develop a model that could be readily employed without substantial cost to investigators. User-friendly refers to the relative ease of use for each subsystem; blast source will need to be easily loaded and detonated, the blast/shock tube should be adjustable (vary length and position, for example) and easy to manipulate, specimen restraints should be easily accessible, and pressure transducers should be easily setup and with relatively easy data readout. Reproducibility means that each aspect should perform the same under the same set of experimental conditions; the factor will play the greatest role in the blast wave source, seeing that consistent blast are vital to the design. Safety of both the operator and the specimen should be taken into consideration; for example, the user's safety is critical when operating the blast source, and the specimen should not receive further damage that a primary blast injury (meaning no blindness or deafness). Construction/maintenance refers to ease of modification and the ability of the object to be

maintained. Below are the options for each subsystem, with a grading under each criterion. A grading scale of 1-3 was used, where 1 did not meet requirements, 2 partially or possibly met requirements, and 3 fully met requirements, thus the higher the score the more favorable the evaluation. Each subsystem contained three alternatives for possible design aspects.

Blast Source

The blast source must be easily reproducible and be able to generate overpressure waves of various strengths. The Hilti tool accepts .22 crimp blanks in a single shot mode. The starter pistol accepts .22 crimp blanks in an 8 shot revolver. The paintball gun generates a compressed air burst using a compressed air tank and a pressure regulator.

Table 2. Options and preliminary ranking for blast source

Option	Cost	User-friendly	Reproducibility	Safety	Construction/ Maintenance	Total
Hilti Tool	**2**	**3**	**3**	**3**	**2**	**13**
Starter Pistol	3	1	3	1	3	11
Paintball Gun	3	1	1	1	1	8

Evaluation of the costs among the three possible blast sources shows that the starter pistol is the least expensive with a cost of around $50 (compared to $200 for the Hilti® tool and $150 for the paintball gun). Because the starter pistol can load eight live rounds at one time, meaning that it will only have to be reloaded once every eight shots, it was rated the best for user-friendliness. The Hilti® tool can only load one round at a time, and the paintball gun can load many rounds at one time but it must constantly be reloaded with compressed air. Because the starter pistol and the Hilti® tool produce a reproducible blast source, which was verified in testing, they rated the highest for reproducibility. However, the paintball gun loses pressure as the compressed air depletes, thus exposing the experiment to additional, unwanted dependent variables. As for safety, two of the sources are guns and one is a power tool. Interestingly, we found that the word “gun” in the name of the item prohibited the use of these items on campus under our University policy on firearms and weapons, so this was factored into the lower safety rating. Nevertheless, the starter pistol can be loaded with the blank powder cartridges and not be loaded (preventing a misfire) whereas the Hilti® tool and the paintball gun are live as soon as the ammunition is placed in the barrel. Finally, the construction and maintenance of the entire apparatus was considered for all blast source devices. Although the all three blast sources cost about the same to construct the apparatus, the starter pistol was the highest rated due to its low maintenance and upkeep cost. The Hilti® tool is expensive to replace parts and, in general, paintball guns require constant upkeep and cleaning in order to maintain them. This analysis thusly concluded that the Hilti® tool is the preferred blast source to be used in future fixture development.

Blast/Shock Tube

The shock tube must be able to withstand the force of multiple blasts without damage. It should also be light, and not generate excessive attenuation or reflection of the overpressure wave. PVC pipe is cheap and resilient, but not as strong. Aluminum pipe is expensive. Steel piping is strong, but heavy harder to build with.

Table 3. Options and preliminary ranking for blast/shock tube

Option	Cost	User-friendly	Reproducibility	Safety	Construction/Maintenance	Total
PVC	**3**	**3**	**3**	**3**	**3**	**15**
Aluminum	2	2	2	3	2	11
Steel	2	2	3	2	2	11

PVC is by far the cheapest option when compared with aluminum and steel piping. It is also lightweight, can be bought in several different dimensions, and is easy to handle which makes it more user-friendly. Due to its fatigue strength of 1.7 megaPascal (MPa) over 10^7 times to an external stress it is also very reproducible, but so is aluminum and steel. For safety purposes all the choices seemed safe. PVC could possibly crack and have a sharp edge, and steel is heavy and could be dangerous if it were to fall. PVC is very easy when it comes to constructing as it can easily be attached to the other devices and is also easy to cut if the size of the tube needs to be varied. Steel is difficult to cut and mill as well as attach to other devices. Maintenance for the three is very similar. They all can be cleaned and kept up with very little effort. After analyzing these criteria we have decided to use PVC for our tubing.

Specimen Restraints

The specimen restraint must be cheap, since multiples will likely be made. Because of the specimens' propensity to defecate and urinate, ease of cleaning and sanitation are important factors. Difficulties in construction will also translate into more expensive restraints, and should be avoided. Wood is easy to work with, but is difficult to clean and sanitize. Plexiglass is easy to work with, and is clear to allow a view of the specimens. Aluminum is expensive and difficult to work with.

Table 4. Options and evaluation for specimen restraints

Option	Cost	User-friendly	Reproducibility	Safety	Construction/ Maintenance	Total

Plexiglas	**3**	**3**	**3**	**3**	**3**	**15**
Wood	3	1	2	1	1	8
Aluminum	1	2	3	2	2	10

After the evaluation of the different options for the specimen restraint we came to the conclusion to use Plexiglas. As far as cost is concerned, both Plexiglas and Wood are very cheap while Aluminum is rather expensive. Plexiglas is also user-friendly because it is easy to assemble and is also 92% transparent, which is the highest transparency of any material.[12] Wood can crack and splinter easily and aluminum is not as easy to cut and handle. All three options can be easily reproduced; the only problem with wood is that if it becomes dirty from the mouse it would have to be replaced. Plexiglas also a very strong resistance to breakage caused by impact (up to 17x that of regular glass). Wood is not safe because of the splintering of the wood. Aluminum also would have sharp edges after cutting and machining that could be a potential problem. The construction of the Plexiglas is also easy to construct because it will be purchased in simple sheets. The maintenance is also simple because Plexiglas can be cleaned easily. Also if the mouse were to urinate and/or defecate the Plexiglas can be simply cleaned and sanitized. The porosity of the wood would not allow for easy clean up. After this analysis it was decided that the best choice for the specimen restraint would be Plexiglas.

Pressure Transducers

The transducers need to be able to output real time data in a way that can be recorded, and be able to be reused easily multiple times. The Honeywell FP2000 configurable pressure transducer is a highly customizable pressure transducer that can output data through a Honeywell circuit for digital readout. Rupture membranes are rudimentary, and must be replaced each time. They cannot provide adequate data at reasonable cost.

Table 5. Options and evaluation for pressure transducers

Option	Cost	User-friendly	Reproducibility	Safety	Construction/Maintenance	Total
PCB Piezoelctronic	**3**	**3**	**3**	**3**	**2**	**14**

Honeywell	1	3	3	3	2	12
Rupture Membrane	3	1	1	3	1	9

The pressure transducers need to be able to output data in real time, so that pressure vs. time data can be graphed. The Honeywell FP2000 configurable pressure transducer ($500) is a highly customizable pressure transducer and is very similar in sampling characteristics and physical size. Similarly, the PCB transducer is an ICP (Integrated Circuit Piezoelectric) Low-Impedance Quartz Pressure Sensor. It has a built in amplifier that converts high impedance charge into a low impedance voltage that is displayed on the oscilloscope. The power to operate the transducer is relatively low cost. It only requires 24-27 VDC and 2-20 mA to run the transducer. The sensor, once mounted, is connected to a constant current signal conditioner. This device maintains a steady amount of voltage and amperes to the device so that the signal is very accurate over the duration of the testing period. The device can also serve as an amplifier in case the signals being read are very small. The oscilloscope is the final piece of the system. This device displays the graph of the wave in Volts/Time. The voltage can then be converted into standard units of pressure using tables that are readily available. Made for versatility in industrial applications, the PCB transducer can be configured to sense from various pressure ports and output data. This transducer has a direct interface into an oscilloscope where data can be stored directly to a USB flash drive. The PCB transducers can detect pressures at the range we plan to test within (100-200 kPa) and read out data at a very high frequency (gigahertz range). These transducers will be used and placed at the same position as the mice head to ensure an accurate overpressure wave striking the specimen. The device selected is the PCB Piezoelctronic transducer Model 101A06. It has a measurement range of ± 5 Volts output with a maximum pressure of 3450 kPa. The transducer has a sensitivity of 1.45mV/kPa. There is a resonant frequency of ≥ 400 kHz. The electrical connection is a 10-32 coaxial jack and the transducer on weighs 12.5 grams. The set-up of the transducer system is illustrated in **Figures 12 and 13**.

Sound Dampening

For the rebounding wave absorber we evaluated different absorptive material to surround 5 faces of a custom built cube. This cube will be constructed using 2'x 2"x1" lumber and lined with hexagonal wire as a support. Inside the cube, there will be a sound dampening device to diffuse and prevent wave reflection. Two different materials were considered: Cascade Pyramid anechoic foam and standard bedding foam.

Table 6. Options and evaluation for rebounding wave absorber

Option	Cost	User-friendly	Reproducibility	Safety	Construction/Maintenance	Total
Cascade	1	2	3	2	2	10

Pyramid						
Bedding Foam	**3**	**2**	**3**	**2**	**2**	**12**

Both of these options are user friendly, safe, and require minimum construction and maintenance. However, the bedding foam is a better choice due to its low cost ($11) compared to the cascade pyramid foam ($160). Due to this high cost difference, the bedding foam was chosen. If fixture tests show that the bedding foam is insufficient/inefficient at preventing reflections, then the Cascade Pyramid foam will be used instead.

Filtering

The raw data obtained from the oscilloscope contains high frequency, low amplitude noise. This obscures the true signal, which consists of high amplitude, high and low frequency data. Because the true signal contains high and low frequency, a simple low-pass filter cannot be used without modification. Instead, separate methods will be used to separate out the true signal in order to preserve both the high amplitude, low frequency signal and the high amplitude, high frequency signal.

Initial X-axis intercept detection

First, a simple moving average low-pass filter is employed to create the smoothest possible curve, with little regard to maintaining peak height. The moving average (MA) filter is a low pass filter with primarily a smoothing effect. Because the moving average filter has a tendency to shift data along the X axis, MA-filtered data is time-shifted to re-align the time position of the peaks. This MA-filtered data is then used to find all the X-axis intercepts, and the indices of these are output.

High-amplitude Pass Filter

Returning to the raw data, a weak low pass Butterworth filter (described in detail later) is employed to increase peak definition. A local maximum and minimum is then found between each X-axis intercept and the value with the highest data being recorded as a local extreme. A simple fit wave is constructed using the X-axis intercepts and the local extremes. The simple fit wave of the high amplitude data is constructed by a linear connection of each of the X-axis intercepts and the local extremes, moving along the X-axis. This high amplitude signal is then subtracted from the raw data, separating the high amplitude signal and leaving a low amplitude signal. Both the high amplitude data and the low amplitude data are output.

Low Pass Filter

Because the high amplitude data is not an ideal curve fit, the low amplitude data still contains low frequency information from the ideal wave which can be extracted. This is done by employing a Butterworth filter. The Butterworth filter is a low pass filter optimized to give a maximally flat frequency response. The resultant data consists of low-frequency data from the true signal.

Reconstruction of the True Signal

The high amplitude data is then added to the low frequency signal to reconstruct the true signal. This data has had all the low amplitude, low frequency data, consisting of the noise, removed. This filtered data represents the best approximation of the true signal.

Graphical User Interface

In order to assist the experimenter in data processing a MATLAB Graphical User Interface (GUI) was developed. A GUI allows the operator to have minimal programming knowledge while still being able to process data. The GUI that we developed is shown below in Figure 8. In order to assist the operator in selecting the data that they want to process, the GUI allows the user to search through the directory for the desired data and select it. After this initial selection, the user then has the option to graphically view the raw data or the filtered data with the time in milliseconds on the x-axis and the pressure generated in kilopascals on the y-axis. Once the user has selected the data, the GUI will output the maximum peak pressure in kilopascals, maximum negative pressure (first negative wave) in kilopascals, and the duration of the wave to the end of the second peak in milliseconds. The filter implemented is the same filter mentioned above (Butterworth). After the user has selected the data and filtered it, they can save it using the "Save Filtered Data" button located at the top of the GUI. This button then saves the filtered data as a separate .csv file for the operator to handle in whatever way they deem fit. Error handling has also been implemented to account for any error that the user develops. An example of the GUI is shown in **Figure 14**. The current fixture design is shown in **Figures 15 and 16**.

Task 7: Determine if single or multiple blast exposures in a mouse confer signs and symptoms similar to those of human mild TBI

This work evaluating a single blast exposure is nearing completion, and a manuscript detailing the results is in preparation. The evaluation of the effects of multiple blast exposures is on-going. With regard to a single blast-overpressure exposure, we previously reported that mice experienced and altered state of consciousness (not extensive loss of consciousness) immediately after the blast-exposure. We also detected acute vestibular motor deficits, but did not observe blast-induced deficis in learning and memory as measured in the acquisition paradigm of the Morris water maze (MWM). We also reported last year that exposure to the blast-overpressure induced increases in state anxiety as measured in the elevated plus maze.

In the current year, we continued the evaluation of the effects of a single blast-exposure on depression/despair using the forced swim task, consumption of food and water in the bioactivity chamber, groom duration as an indicator of compulsive behavior, and duration of immobility in the light and dark cycle as an evaluation of sleep/insomina. We evaluated the effect of impact-acceleration (weight drop injury) or blast-induced brain injury on depression/despair-like behaviors as measured using the forced swim task. Animals are placed in a 4L beaker of water and recorded for 6 minutes of swimming. To score the task, the time spent immobile was determined in minutes 2 – 6, with longer immobility times indicating increased depression or despair. As seen in **Figure 17**, animals that were exposed to the blast had increased immobility time as compared to the sham and weight drop groups. These data suggest that blast-induced brain injury induced depression/despair. Another set of experiments were conducted in bioactivity chambers. The bioactivity chamber utilized was the LABORS system as described for task 3. For these experiments, mice were individually housed and evaluated using the LABORAS monitoring system (Metris, Inc.). The LABORAS is a non-invasive behavioral monitoring system that automatically recognizes and quantifies several normal and abnormal behaviors of mice (**Figure 9**). For these experiments, mice were placed in

the home cage in the LABORAS monitoring system for 5 days to obtain baseline behaviors. Then mice were randomly assigned to either sham, blast-induced, or impact-induced mTBI groups. One hour after the induction of the brain injury (or sham), mice were returned to the LABORAS home-cage and monitored for a subsequent 6 days post-TBI. Although the data analysis from the vast set of data obtained from the LABORAS system are currently being evaluated, preliminary data suggest the impact- or blast-induced mTBI induce differences in home cage behaviors. For example, resting or immobility is defined as a period when movement is absent while the animal is in a sitting or lying position. With regard to food and water consumption, animals had free access to food and water and the average total food consumption before and after TBI are shown in **Figure 18**. No differences were observed between sham and weight drop groups, however a trend was observed to have less food consumption after mTBI. To measure activity and sleep, the immobility duration during the light and dark cycle were examined. As seen in **Figure 19**, in both the day (typically less active cycle; panel A) and night (typically more active cycle; panel B) mice that received a blast-induced TBI exhibited reduced numbers of immobility instances than mice in the sham or impact-induced mTBI groups, which suggest insomnia-like behaviors. Grooming duration, a measure of active activity, is defined as the time the mouse spends shaking, scratching, or wiping/ licking its fur, snout, ears, tail, or genitals. As seen in **Figure 20**, in the day (panel A) mice that received either an impact-induced or blast-induced mTBI increased the grooming duration as compared to shams. In the night (panel B) mice that received an mTBI increased the duration of grooming as compared to shams and mice in the impact-induced mTBI group trended toward greater increases in grooming duration than mice in the blast-induced group. Preliminarily these data suggest that blast-induced mTBI reduces the sleep of mice and induces excessive grooming. Impact-induced mTBI does not appreciably alter the sleep cycle of mice, but also induces excessive grooming. Excessive grooming in mice has been associated with alterations in cognition including hyperactivity, anxiety, obsessive compulsive-like disorder, and has also been associated with increased in sensory sensitivity and/or pain.

Task 8: Evaluation/ optimization of fixture construction, load generation of mouse blast apparatus

Loading data was provided to UA by UAB. Information related to curve fitting the data to a blast model was provided by UA by first importing the data into a spreadsheet format. Then, the curve fit mechanism was added in computational form so that the user could do a visual curve fit in order to observe the impact of changing the two important parameters, alpha and beta, on the curve fit in terms of the peak overpressure and the underpressure. Furthermore, sample calculations and a mechanism for curve fitting other data in an effective manner were provided via e-mail of this spreadsheet and then subsequently incorporated into the GUI described above. Our model we have recently developed induces a highly reproducible blast wave that includes both the static overpressure and underpressure components of the Freidlander function with a highly reproducible reflective amplication to result in a reproducible complex wave. As seen in **figure 21,** independent replications (run 1 and 2) induced nearly identical blast waveforms. These blast waves rapidly reach a peak overpressure (26 psi) and are followed by a rapid underpressure which closely fits a Friedlander function (pink line). Additionally, the

chamber characteristics are such that reproducible reflections occur making this a complex blast wave, similar to that potentially experienced in the battlespace.

Task 9: Evaluate the cortex, hippocampus, thalamus, cerebellum, and amygdala of mice exposed to single or multiple sub-lethal blast exposure for pathological indicators of brain trauma

This work is nearing completion, but is still ongoing. All tissue specimens have been processed and quantification of markers of cell injury is continuing. New data include histochemistry and example micrographs from brain sections processed with immunohistochemistry to detect diffuse axonal damage and white matter damage are shown. Serial sections throughout the mouse brain were evaluated by an investigator naïve to the treatment condition of the animal and a damaged axon that had a clear morphological disruption or retraction ball was counted if the APP-positivity was at least 2X background. As seen in **Figure 22**, immunohistochemistry to evaluate accumulation of amyloid precursor protein (APP) in axons showed that both the impact-induced and blast-induced mTBI groups had substantially more APP+ axons than the sham group. These data are being completed but preliminary analysis indicates that diffuse axonal injury occurs in both injury modalities. In a sister set of serial sections, we processed the tissue with an antibody against myelin basic protein (MBP) to visualize white matter damage (**Figure 23**). Sections throughout the brains were ranked by an investigator who was naïve the treatment of the animal. The ranking was as follows: 0=no damaged myelin; 1= some damaged myelin; and 2= extensive damaged myelin. As shown by the rankings, on average some damaged myelin was observed after weight drop or blast-induced mTBI.

Key Research Accomplishments:

- Estimation of the static compression results that produce some permanent deformation of MT
- Modeling of pressure wave propagation through the MT and calculation of stress as related to yield strength
- Prediction of blast-induced permanent damage to the MT
- Estimate of resulting stresses in the cytoplasm, based on the assumed geometry, and comparison to stresses in MT
- Estimation of Von Mises under various load conditions
- Evaluation of 0.588 J impact-acceleration injury in adult male mice with regard to duration of transient unconsciousness, vestibular motor performance, alterations in learning and memory, and effects on insomnia, anxiety, depression, and compulsive-like behaviors.
- Design, and prototyping of mouse blast fixture using a commercially available detonation source
- Evaluation of head only blast exposure in adult male mice with regard to duration of transient unconsciousness and alterations in consciousness, vestibular motor performance, alterations in learning and memory, and effects on insomnia, anxiety, depression, and compulsive-like behaviors.
- Evaluation of histological markers of injury after head only blast exposure

Reportable Outcomes:

- Abstract: Biao B. (Bill) Zhang and W. Steve Shepard Jr., Candace L. Floyd. Investigation of stress wave propagation in brain tissues through the use of finite element method. ASME 2010
- Abstract: Tracy Niedzielko and Candace Floyd. Comparison of blast- and impact-induced mild traumatic brain injury in adult male mice. National Neurotrauma Society 2011.

Conclusion:

Modeling research in the past year has continued to focus on identifying the important issues that must be addressed to understand the complex loading provided by the AFM tip for the *in vitro* loading as well as the transient loading produced by a propagating pressure wave. Because of the complex nature of the AFM loading, several different models have been utilized to help gain a better understanding of the important characteristics of that loading. Note that this correlation study with the AFM loading only examines static considerations. Current studies involve correlating the stresses obtained in that static model to those stresses obtained in the dynamic wave propagation studies, which will provide a better understanding of how blast overpressure impacts the MT structure. Not only will the *in vitro* condition be modeled, but the *in vivo* conditions that a MT would experience in a brain are also being examined for both static and transient conditions. Although preliminary transient wave propagation models are complete, studies on the resulting microstructure response, such as stresses, are currently being examined.

The model used to simulate the microstructure within the brain, the CSE model, was initially used to shed insight on the impact of nearby microtubules. That simulation showed that stresses begin to increase as the distance between MTs decreases below 80 nm. Furthermore, since it is known that the relative MT spacing provided by the motor proteins is approximately 10 to 20 nm, the expected stresses within the MT will be higher when a motor protein has joined two MTs or a MT is jointed to some other structure.

It should also be noted that three presentations of the work were made this year. One presentation of the paper, related to the abstract given in last year's annual report, was made at the ASME IMECE2010 in Vancouver in November. Then, in March, a presentation of the research was made at The University of Alabama's Mechanical Engineering Graduate Student Symposium. Finally, a presentation was made to Ms. Karen Garrison's Anatomy and Physiology classes at Tuscaloosa County High School. This last presentation was given to two classes. Note that another presentation of the work, related to the Abstract listed in this year's report (see below), will be made at IMECE 2011 in Denver. In addition, a summary of the in vivo work thus far was presented at the National Neurotrauma Society Annual meeting in July 2011 and a manuscript is under preparation.

References:

1. A. G. Gross, "Impact thresholds of brain concussion," *J. Aviation Med.*, **29**(10), pp. 725-732 (1958).
2. A. K. Ommaya, P. Yarnell, A. E. Hirsch and E. H. Harris, "Scaling of experimental data on cerebral concussion in sub-human primates to concussion threshold for man," *in Proceedings of 11th Stapp Car Crash Conference* (New York, 1967) 670906, pp. 47-52.
3. Y. K. Liu and K. B. Chandran, "The exact solution for the translational acceleration of fluid-filled rigid spherical shells - A model for the development of intracranial pressure," *Mathematical Biosciences*, **24**, pp. 1-16 (1975).
4. G. T. Fallenstein, V. D. Hulce and J. W. Melvin, "Dynamic mechanical properties of human brain tissue," *J. Biomechanics*, **2**(3), pp. 217-226 (1969).
5. J. E. Galford and J. H. McElhaney, "Some viscoelastic properties of scalp, brain, and dura," *in Proceedings of ASME Meeting 69-BHF-7* (Ann Arbor, MI, 1969), pp. 8.
6. M. Sato, W. A. Schwartz, S. C. Selden and T. D. Pollard, "Mechanical properties of brain tubulin and microtubules," *J. Cell. Bio.*, **106**(4), pp. 1205-1211 (1988).
7. J. A. Galbraith, L. E. Thibault and D. R. Matteson, "Mechanical and electrical responses of the squid giant axon to simple elongation," *J. Biomech. Eng.*, **115**(1), pp. 13-22 (1993).
8. B. R. Donnelly and J. Medige, "Shear properties of human brain tissue," *J. Biomech. Eng.*, **119**(4), pp. 423-432 (1997).
9. K. Miller, K. Chinzei, G. Orssengo and P. Bednarz, "Mechanical properties of brain tissue in-vivo: experiment and computer simulation," *J. Biomechanics*, **33**(11), pp. 1369-1376 (2000).
10. B. Fabry, G. N. Maksym, J. P. Butler, M. Glogauer, D. Navajas and J. J. Fredberg, "Scaling the microrheology of living cells," *Physical Rev. Letters*, **87**(14), pp. 148102-1-4 (2001).
11. K. Miller and K. Chinzei, "Mechanical properties of brain tissue in tension," *J. Biomechanics*, **35**(4), pp. 483-490 (2002).
12. M. Shafieian and K. Darvish, "Effect of TBI on material properties of rat brain tissue," *in Proceedings of 33rd Annual Northeast Bioengineering Conference, NEBC* (Stony Brook, NY, 2007), pp. 283-284.
13. M. A. Green, L. E. Bilston and R. Sinkus, "In vivo brain viscoelastic properties measured by magnetic resonance elastography," *NMR Biomed.*, **21**(7), pp. 755-764 (2008).
14. J. S. Ruan, T. Khalil and A. I. King, "Dynamic response of the human head to impact by three-dimensional finite element analysis," *J. Biomech. Eng.*, **116**(1), pp. 44-50 (1994).
15. R. Willinger, H.-S. Kang and B. Diaw, "Three-dimensional human head finite-element model validation against two experimental impacts," *Annals Biomedial Eng.*, **27**(3), pp. 403-410 (1999).
16. Y. H. Chu and M. Bottlang, Finite element analysis of traumatic brain injury, Tenth Annual Symposium on Computational Methods in Orthopaedic Biomechanics, (2002).
17. C. S. Cotter, P. K. Smolarkiewicz and I. N. Szczyrba, "A viscoelastic model for brain injuries," *Int. J. Num. Meth. Fluids*, **40**(1-2), pp. 303-311 (2002).
18. S. Kleiven and W. N. Hardy, "Correlation of an FE model of the human head with local brain motion - Consequences for injury prediction," *Stapp Car Crash Journal*, **46**, pp. 123-144 (2002).
19. C. M. Suh, S. H. Kim and W. Goldsmith, "Finite element analysis of brain injury due to head impact," *Int. J. Mod. Phys. B*, **79**(8-9), pp. 1355-1361 (2003).
20. S. Kleiven, "Evaluation of head injury criteria using a finite element model validated against experiments on localized brain motion, intracerebral acceleration, and intracranial pressure," *I. J. Crash.*, **11**(1), pp. 65-79 (2006).
21. H. Mao, L. Zhang, K. H. Yang and A. I. King, "Application of a finite element model to the brain to study traumatic brain injury mechanisms in the rat," *Stapp Car Crash Journal*, **50**, pp. 583-600 (2006).
22. J. Ho and S. Kleiven, "Dynamic response of the brain with vasculature: A three-dimensional computational study," *J. Biomechanics*, **40**(13), pp. 3006-3012 (2007).
23. H. Zou and J. P. Schmiedeler, "Predicting brain injury under impact with a strain measure from analytical models," *I. J. Crash.*, **13**(3), pp. 337-348 (2008).
24. T. A. Gennarelli, "Mechanisms of brain injury," *J. Emerg. Med.*, **11**(Suppl. 1), pp. 5-11 (1993).
25. B. Morrison, III, H. L. Cater, C. C. B. Wang, F. C. Thomas, C. T. Hung, G. A. Ateshian and L. E. Sundstrom, "A tissue level tolerance criterion for living brain developed with an in vitro model of traumatic mechanical loading," *Stapp Car Crash Journal*, **47**, pp. 93-105 (2003).
26. L. Zhang, K. H. Yang, A. I. King and D. C. Viano, A new biomechanical predictor for mild traumatic brain injury - a preliminary finding, Summer Bioengineering Conference, (2003).

27. L. Zhang, K. H. Yang and A. I. King, "A proposed injury threshold for mild traumatic brain injury," *J. Biomech. Eng.*, **126**(2), pp. 226-236 (2004).
28. K. H. Taber, D. L. Warden and R. A. Hurley, "Blast-related traumatic brain injury: What is known?," *J. Neuropsychiatry Clin Neurosci*, **18**(2), pp. 141-145 (2006).
29. S. Kleiven, "Biomechanics and thresholds for mTBI in humans," *in Proceedings of IBIA Congress* (Lisbon, Portugal, 2008),
30. S. G. Waxman, J. D. Kocsis and P. K. Stys, The Axon: Structure, Function, and Pathophysiology, p. 692 (1995).
31. A. Brown, "Slow axonal transport: stop and go traffic in the axon," *Nat. Rev. Mol. Cell Biol.*, **1**(2), pp. 153-156 (2000).
32. D. A. Fletcher and R. D. Mullins, "Cell mechanics and the cytoskeleton," *Nature*, **463**(7280), pp. 485-492 (2010).
33. A. Peters and J. E. Vaughn, "Microtubules and filaments in the axons and astrocytes of early postnatal rat optic nerves," *J. Cell. Bio.*, **32**(1), pp. 113-119 (1967).
34. A. Livingston, "Microtubules in myelinated and unmyelinated axons of rat sciatic nerve," *Cell Tiss. Res.*, 182(3), pp. 401-407 (1977).
35. F. Gittes, B. Mickey, J. Nettleton and J. Howard, "Flexural rigidity of microtubules and actin filaments measured from thermal fluctuations in shape," *J. Cell. Bio.*, **120**(4), pp. 923-934 (1993).
36. M. Elbaum, D. K. Fygenson and A. Libchaber, "Buckling microtubules in vesicles," *Physical Rev. Letters*, **76**(21), pp. 4078-4081 (1996).
37. H. Felgner, R. Frank and M. Schliwa, "Flexural rigidity of microtubules measured with the use of optical tweezers," *J. Cell Sci.*, **109**(2), pp. 509-516 (1996).
38. A. Vinckier, C. Dumortier, Y. Engelborghs and L. Hellemans, "Dynamical and mechanical study of immobilized microtubules with atomic force microscopy," *J. Vac. Sci. Technol. B*, **14**(2), pp. 1427-1431 (1996).
39. A. Kis, S. Kasas, B. Babic, A. J. Kulik, W. Benoit, G. A. D. Briggs, C. Schonenberger, S. Catsicas and L. Forro, "Nanomechanics of microtubules," *Physical Rev. Letters*, **89**(24), pp. 248101-1-4 (2002).
40. P. J. de Pablo, I. A. T. Schaap, F. C. MacKintosh and C. F. Schmidt, "Deformation and collapse of microtubules on the nanometer scale," *Physical Rev. Letters*, **91**(9), pp. 098101-1-4 (2003).
41. I. A. T. Schaap, P. J. de Pablo and C. F. Schmidt, "Resolving the molecular structure of microtubules under physiological conditions with scanning force microscopy," *Eur. Biophys. J.*, **33**(5), pp. 462-467 (2004).
42. C. P. Brangwynne, F. C. MacKintosh, S. Kumar, N. A. Geisse, J. Talbot, L. Mahadevan, K. K. Parker, D. E. Ingber and D. A. Weitz, "Microtubules can bear enhanced comrpessive loads in living cells because of lateral reinforcement," *J. Cell. Bio.*, **173**(5), pp. 733-741 (2006).
43. I. A. T. Schaap, C. Carrasco, P. J. de Pablo and F. C. MacKintosh, "Elastic response, buckling, and instability of microtubules under radial indentation," *Biophysical J.*, **91**(4), pp. 1521-1531 (2006).
44. D. Sept and F. C. MacKintosh, "Microtubule elasticity: Connecting all-atom simulations with continuum mechanics," *Physical Rev. Letters*, **104**(1), pp. 018101-1-4 (2010).
45. K. K. Darvish and J. R. Crandall, "Nonlinear viscoelastic effects in oscillatory shear deformation of brain tissue," *Med. Eng. & Phys.*, **23**(9), pp. 633-645 (2001).
46. P. A. Janmey, U. Euteneuer, P. Traub and M. Schliwa, "Viscoelastic properties of vimentin compared with other filamentous biopolymer networks," *J. Cell. Bio.*, **113**(1), pp. 155-160 (1992).

Appendices: Abstracts

Investigation of stress wave propagation in brain tissues through the use of finite element method

Biao B. (Bill) Zhang and W. Steve Shepard Jr.
Dept. of Mechanical Engineering, The University of Alabama , Box 870276 , Tuscaloosa, AL 35487
Candace L. Floyd
Dept. of Physical Medicine & Rehabilitation , The University of Alabama at Birmingham , Birmingham , AL 35249

Because axons serve as the conduit for signal transmission within the brain, research related to axon damage during brain injury has received much attention in recent years. Although myelinated axons appear as a uniform white matter, the complex structure of axons has not been thoroughly considered in the study of fundamental structural injury mechanisms. Most axons are surrounded by an insulating sheath of myelin. Furthermore, hollow tube-like microtubules provide a for m of structural support as well as a means for transport within the axon. There are also discontinuous neurofilaments that serve to strengthen and maintain the axon shape. In this work, the effects of some of these elements on the axon structure are considered in order to obtain a better understanding of wave propagation within the axon. Brain tissues must often be described using complex properties, like viscoelastic or hyperelastic materials, and are often not well characterized. Nevertheless, a means for dealing with some of these issues is considered in an attempt to make progress in this area of brain injury modeling. The goal is to examine axial wave propagation using a simplified finite element analysis so that the impact caused by blast wave loads within the brain axons can be better understood. By conducting a transient analysis, stress and strain distributions as the wave propagates are examined and important characteristics studied. Supported by: DoD CDMRP W81XWH-08-1-0289

Comparison of blast- and impact-induced mild traumatic brain injury in adult male mice.
Tracy Niedzielko and Candace L. Floyd
Department of Physical Medicine and Rehabilitation
University of Alabama, Birmingham

Approximately 1.7 million people acquire a traumatic brain injury (TBI) every year in the US with approximately 75% classified as mild traumatic brain injury (mTBI). Mild TBI can be caused from a large array of events including falls, car accidents, acts of violence, and recently of interest, exposure to blast waves due to explosions. However, it remains unclear if the pathophysiology of blast-induced mTBI differs from that of impact-induced mTBI. Consequently, the goal of this study was to compare the behavioral effects incurred in a blast model of mTBI with those of an impact acceleration model of mTBI. Adult, C57BL/6 mice were randomly assigned one of the following groups 1) sham uninjured controls 2) blast-induced mTBI or 3) impact-induced mTBI. Motor function, learning and memory, anxiety, depression/despair, and ethological behaviors were assessed using the following behavior tasks: Rotorod, Morris water maze, elevated plus maze, forced swim, and the Laboras bioactivity chamber. No significant differences between groups were observed on motor function or learning and memory tasks. Blast-induced mTBI increased anxiety and depression/ despair behaviors over both sham and impact-induced groups. Blast-induced mTBI animals also

exhibited an increase in overgrooming in the light and dark cycles, which is an indicator of obsessive compulsive- like behavior. Also, mice in the blast-induced mTBI group exhibited an increase in locomotion during the dark cycle as compared to both sham and impact-induced mTBI groups. These data indicate that while blast may not cause impairment in locomotor function and learning and memory, it may induce changes in anxiety, depression, and ethological behaviors indicative of obsessive compulsive disorder and insomnia. Supported by W81XWH-08-1-0289.

Table 1 Microtubule material properties

1	MAT Density	1040	kgm^{-3}
2	MAT Poisson's ratio	0.499	-
3	MAT young's modulus	1000	Nm^{-2}
3	MT density	1040	kgm^{-3}
4	MT Poisson's ratio	0.3	-
5	MT young's modulus	2.2	Nm^{-2}

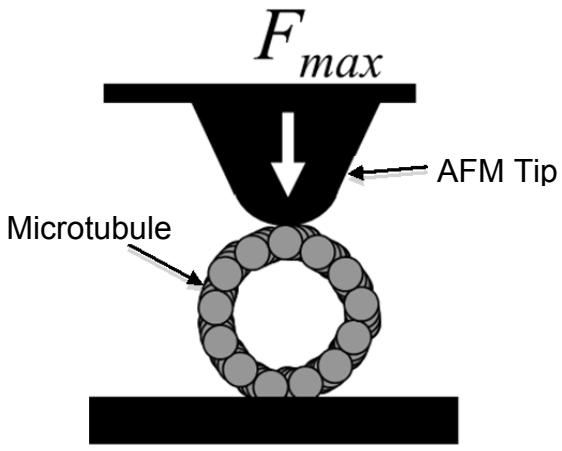

Figure 1. Illustration of AFM experiments on microtubule structure like those done in (12).

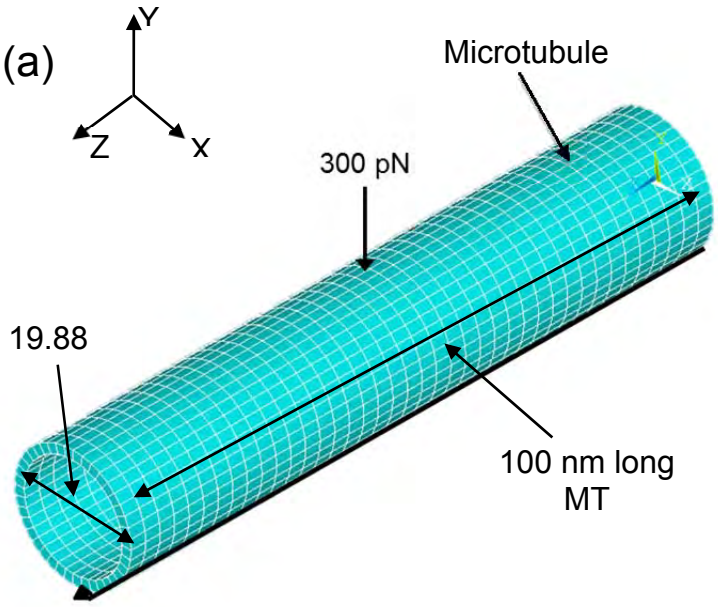

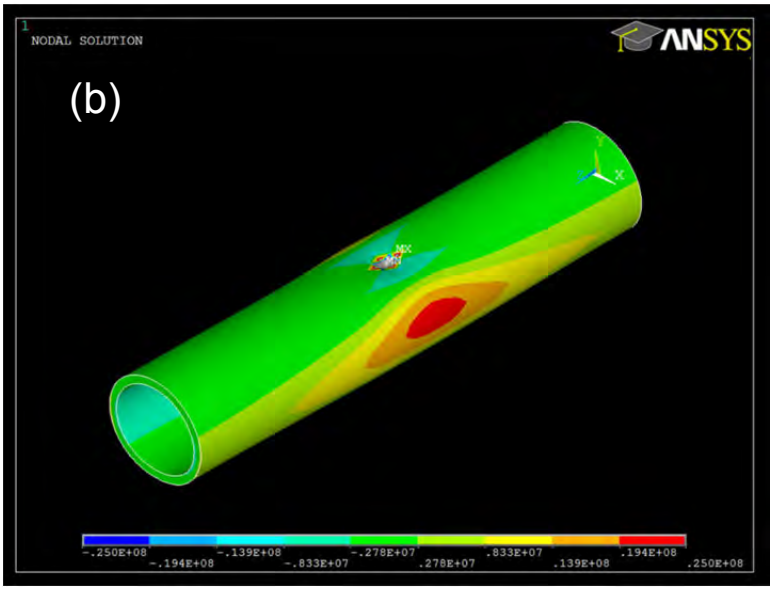

Figure 2 (a). Point Load (PL) model with 300 pN static radial point load. (b). Y-stress distribution of PL model.

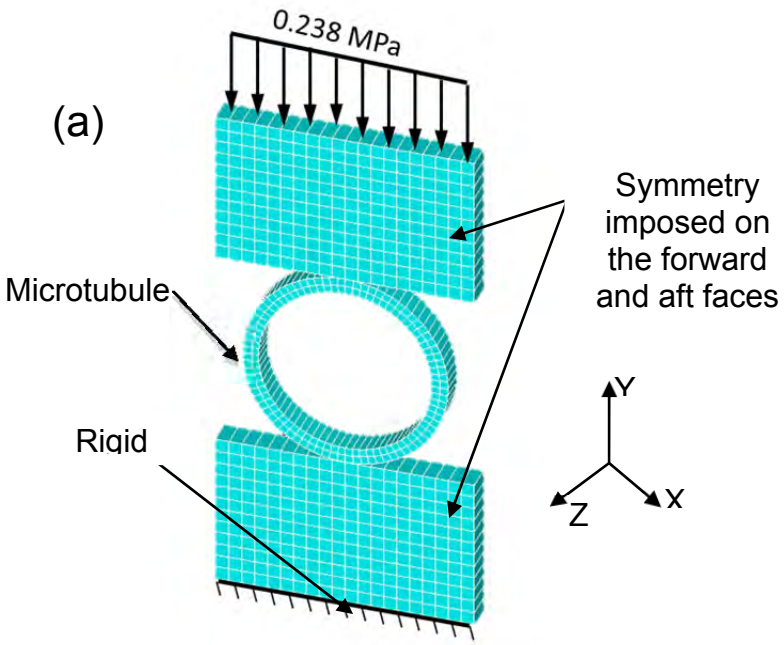

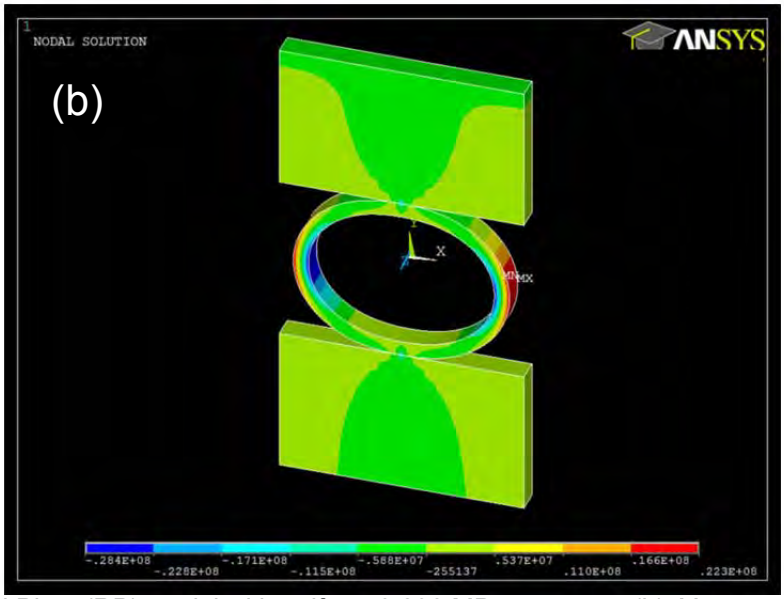

Figure 3 (a). Rigid Plate (RP) model with uniform 0.238 MPa pressure. (b). Y-stress distribution of RP model.

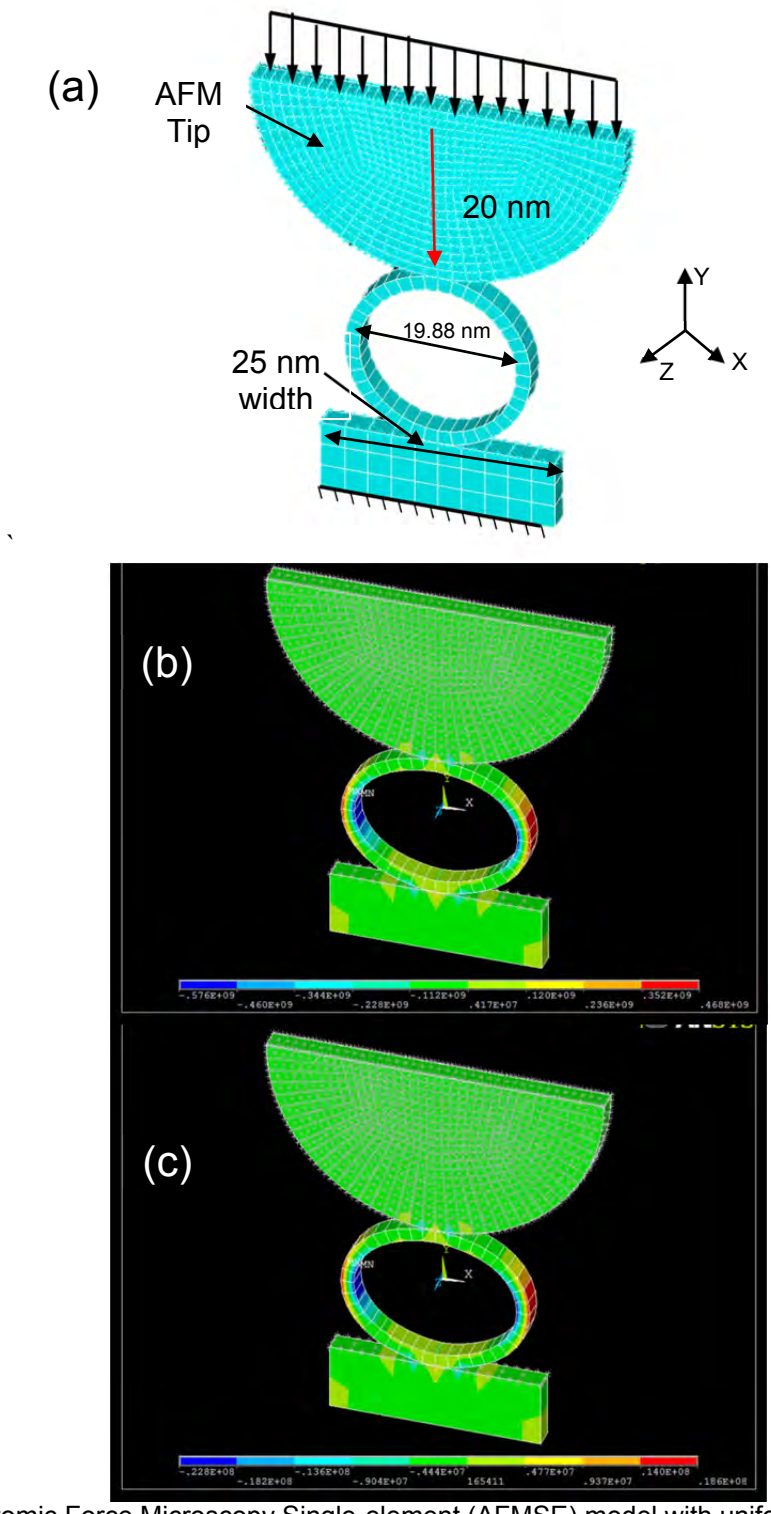

Figure 4 (a). Atomic Force Microscopy Single-element (AFMSE) model with uniform 3.75 MPa pressure. (b). Y-stress distribution of AFMSE model with 3.75 MPa load. (c). Y-stress distribution of AFMSE model with 0.182 MPa load.

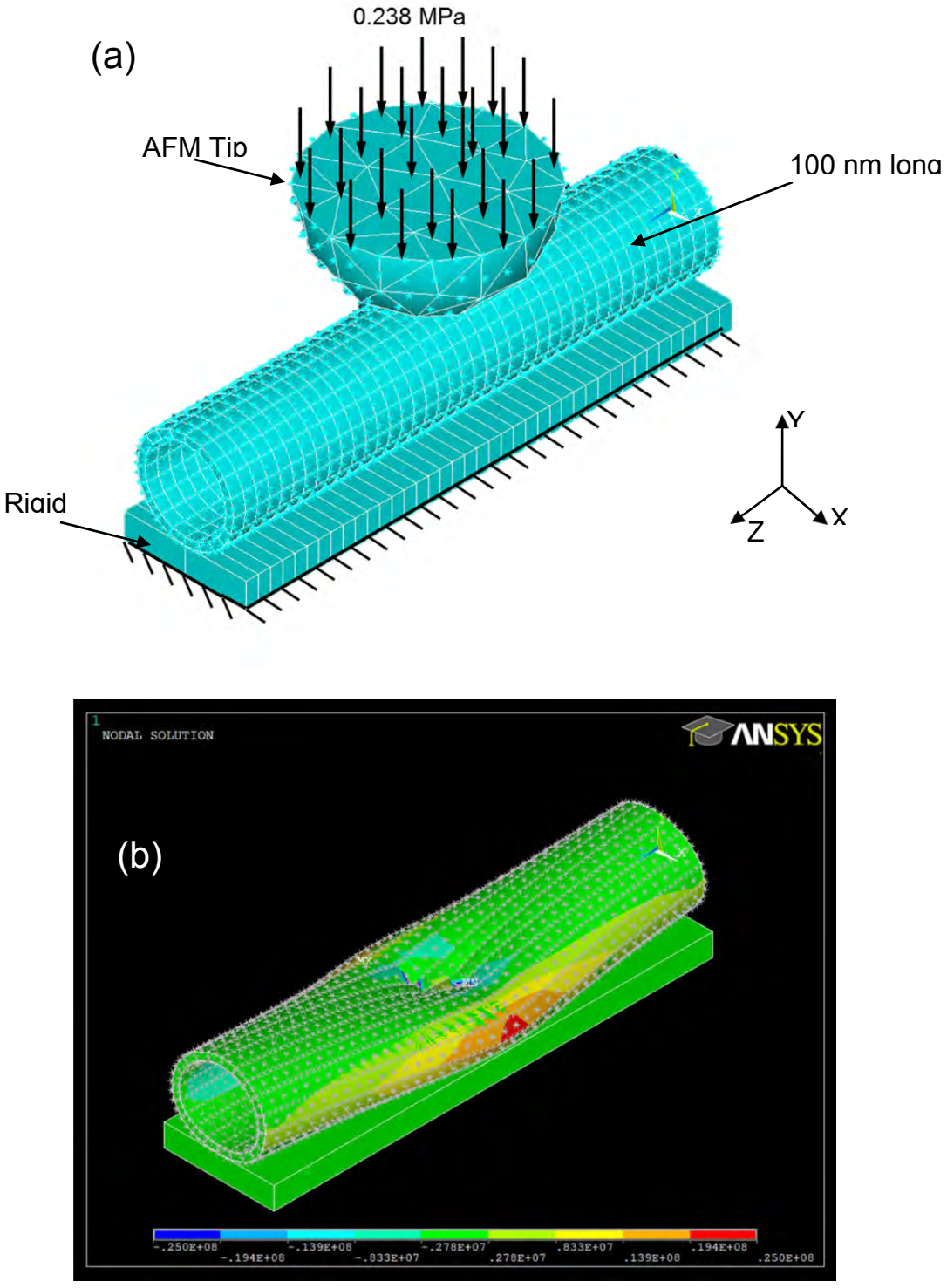

Figure 5. (a). Atomic Force Microscopy Full (AFMF) model with uniform 0.238 MPa pressure. (b). Y-stress distribution of AFMF model with 0.238 MPa load.

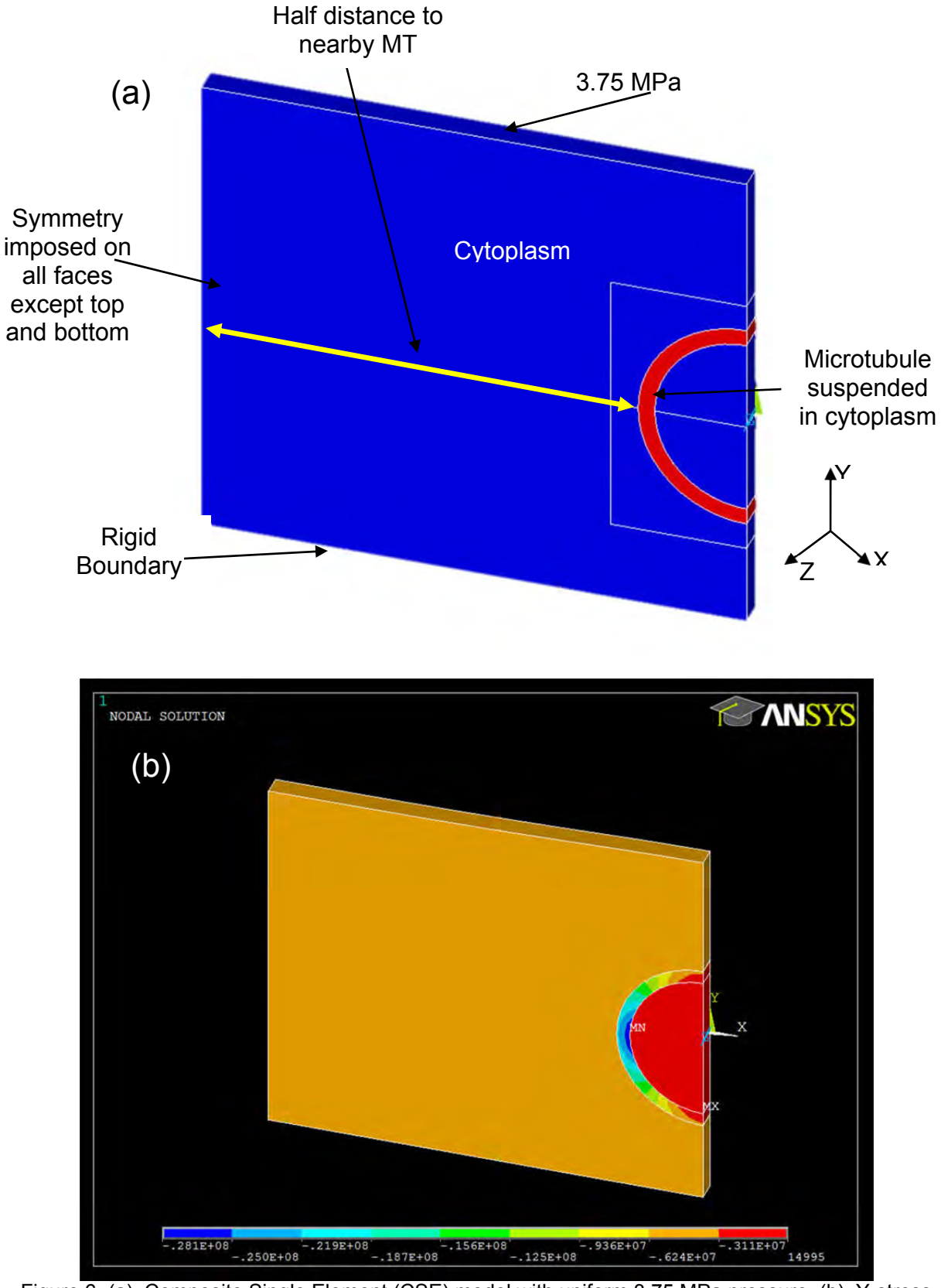

Figure 6 (a). Composite Single Element (CSE) model with uniform 3.75 MPa pressure. (b). Y-stress distribution of CSE model with 3.75 MPa load.

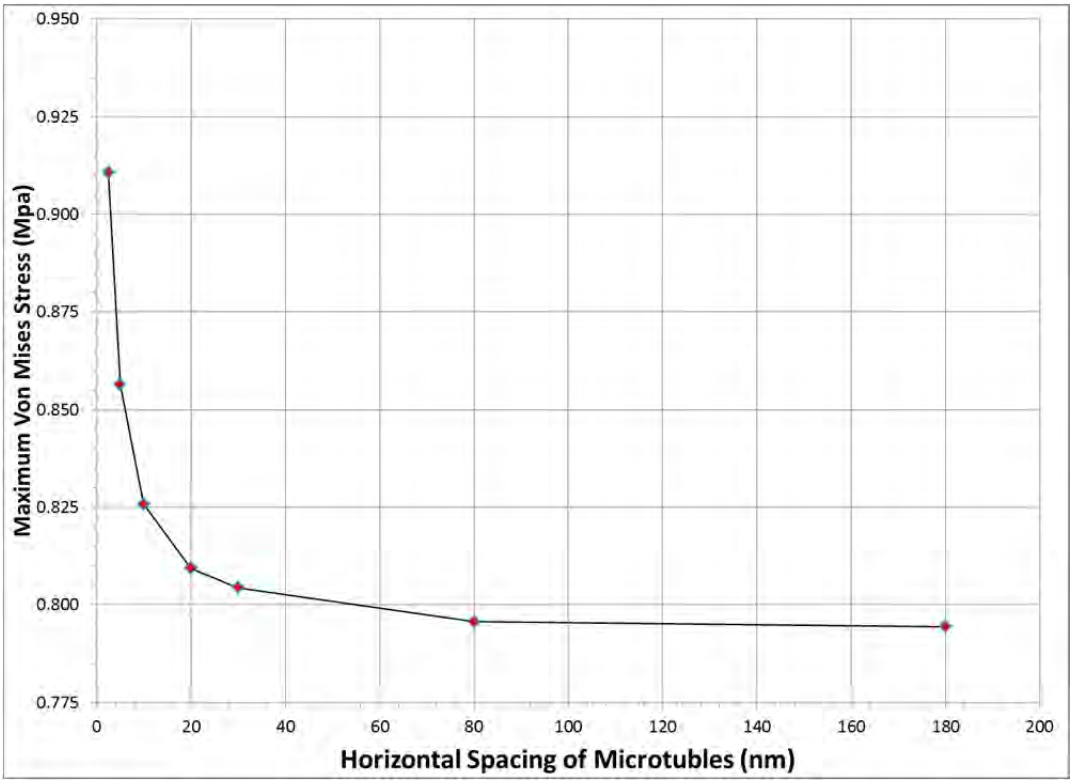

Figure 7. Impact of horizontal spacing of MTs on maximum von Mises stresses.

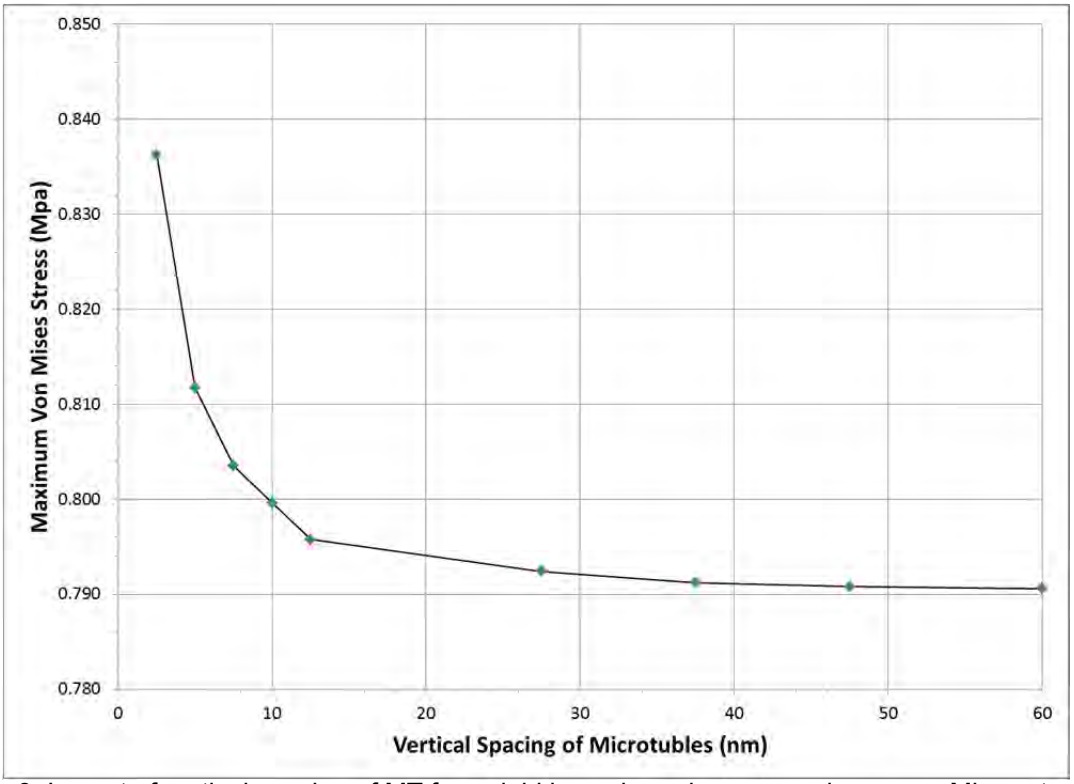

Figure 8. Impact of vertical spacing of MT from rigid lower boundary on maximum von Mises stresses.

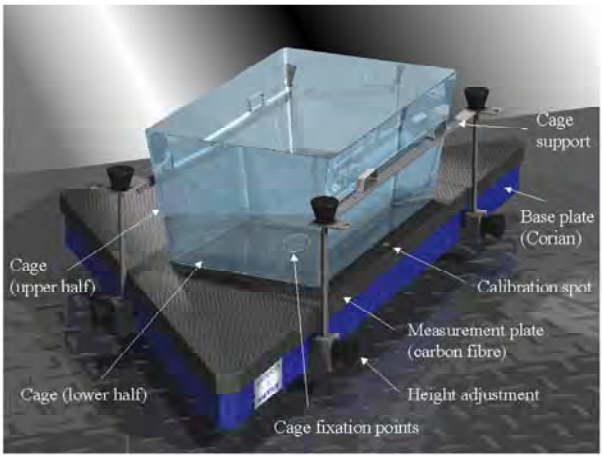

Figure 9: LABORAS behavioral analysis cage. Images is from manufacturer's information (Metris, Inc.) http://www.metris.nl/laboras/laboras.htm. Activity of the mouse can be measured in non-invasive home-cage environment.

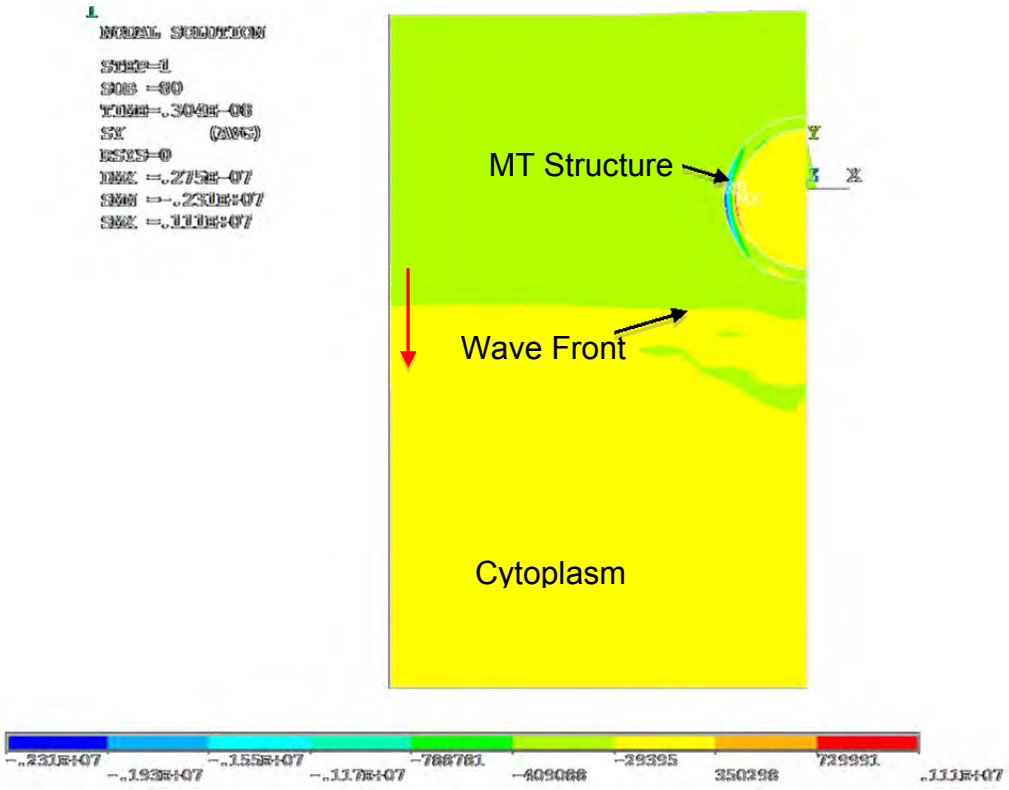

Figure **10:** Sample results for dynamic wave propagation model shown with wave just below MT bottom.

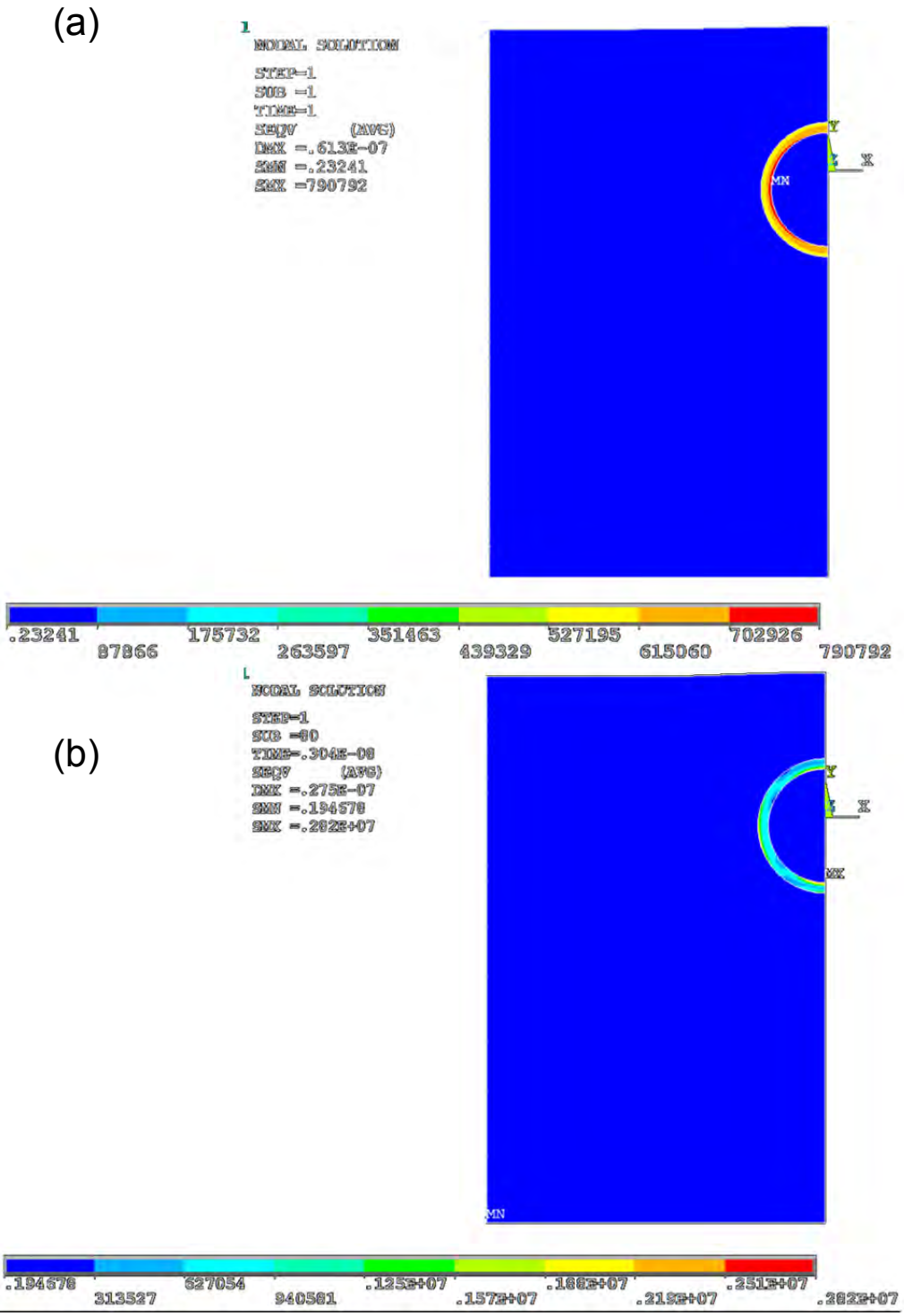

Figure 11. Preliminary transient study comparison, (a) maximum stresses in static loading model, and (b) maximum stresses in transient loading model (different scales).

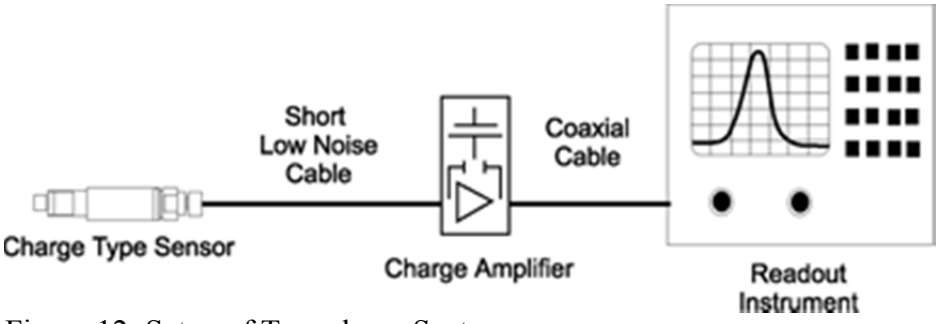

Figure 12: Setup of Transducer System

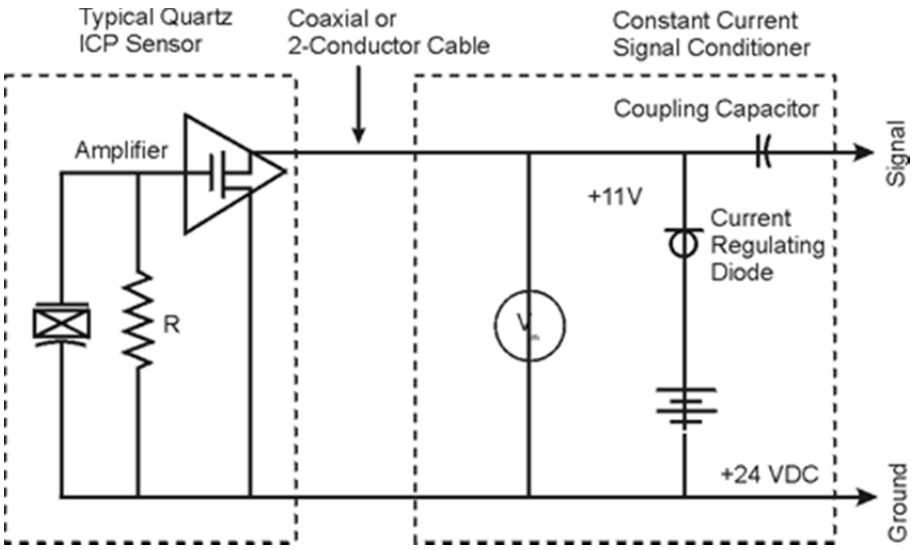

Figure 13: Circuit of the Transducer and Constant Current Signal Conditioner

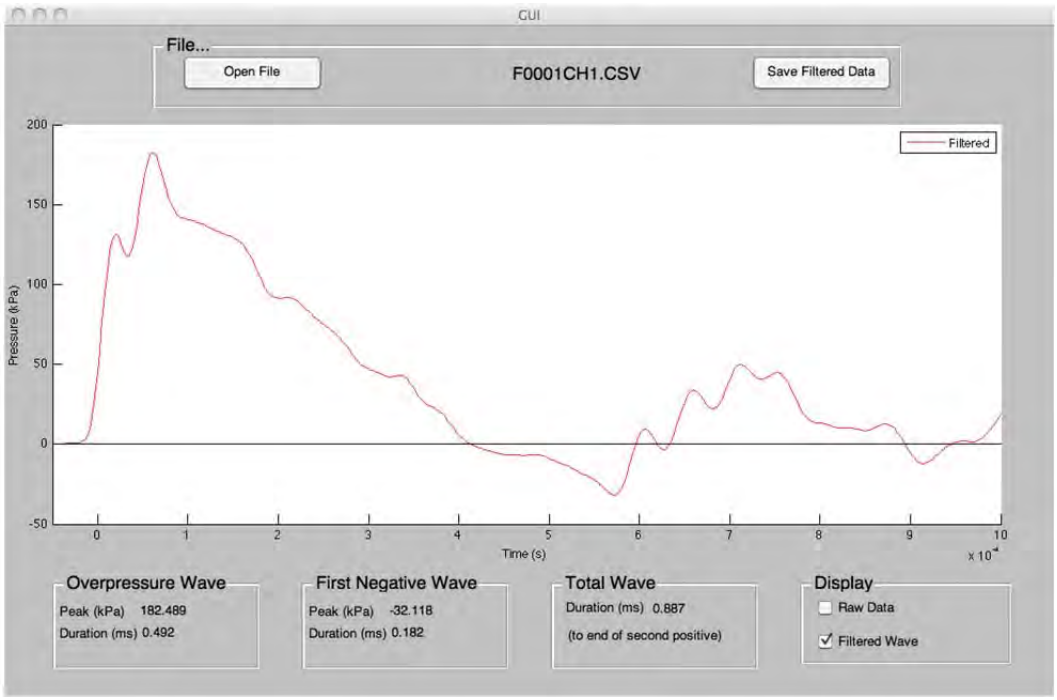

Figure 14: MATLAB GUI to assist the operator in processing data

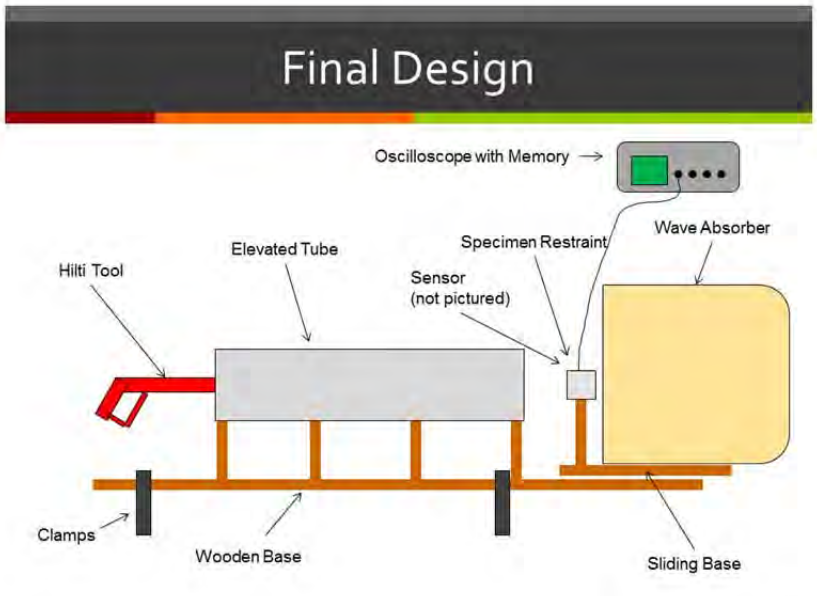

Figure 15: Diagram of parts of test system fixture for final (current) design

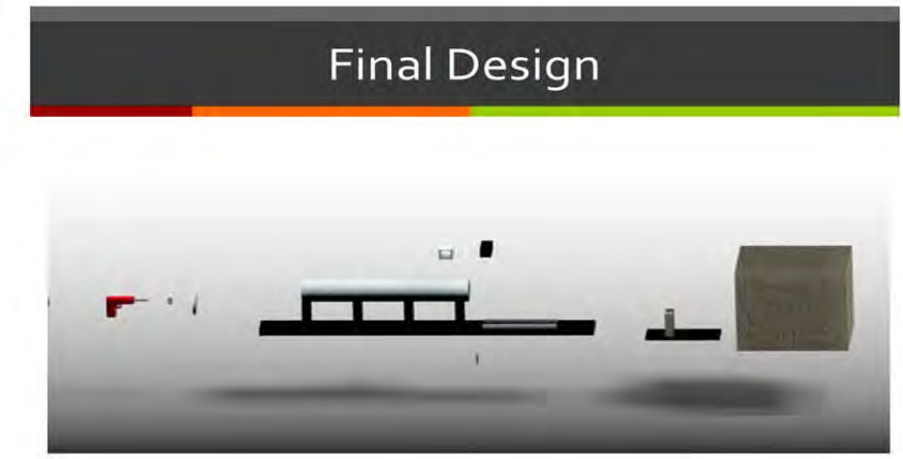

Figure 16 : Computer-assisted 3-D scale model of test system fixture for final (current) design.

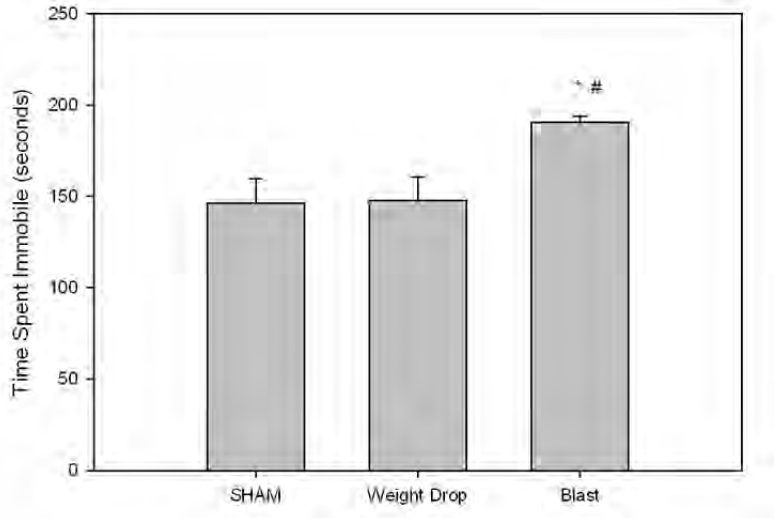

Figure 17: Measuring depression/despair using the Forced Swim task.
The blast group had significantly greater immobility time as compared to the weight drop group (indicated by #).

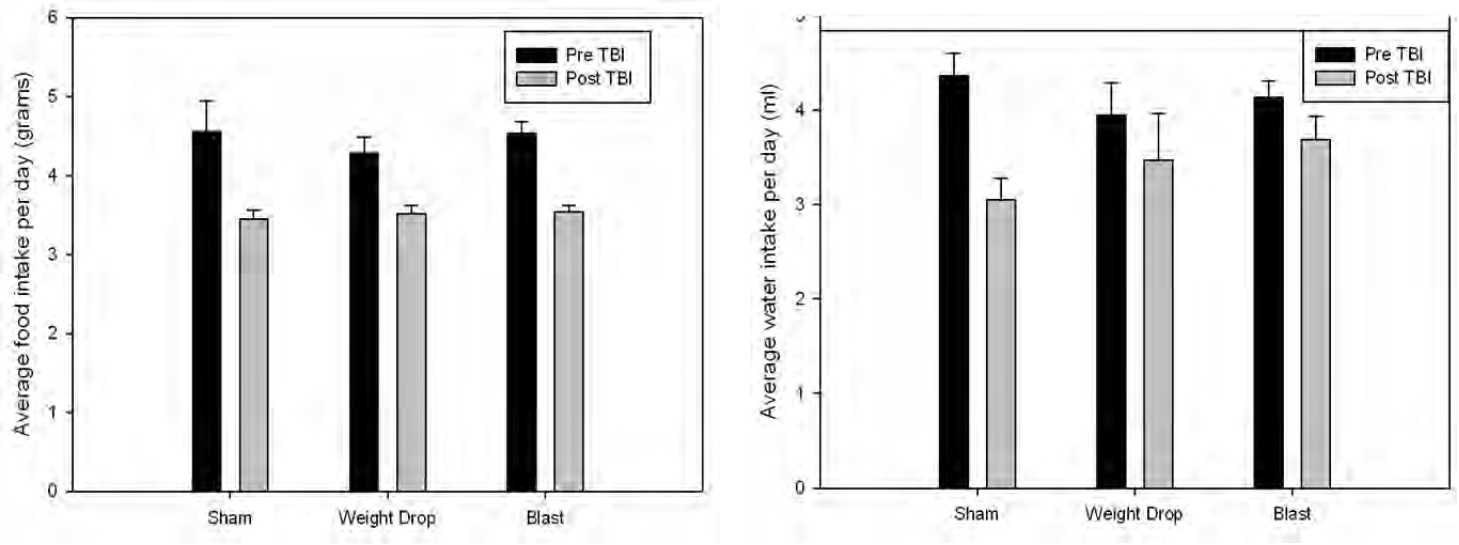

Figure 18: The animals were placed in the Laboras bioactivity chambers for day -5 to day 0 pre mTBI and days 0-6 post mTBI. Animals had free access to food and water. Food and water consumption was tracked during the course of the time spent in the chambers. There is no significant difference between groups in both the food and water between all groups, although there is a trend towards consumption of less food and water post mTBI in all groups.

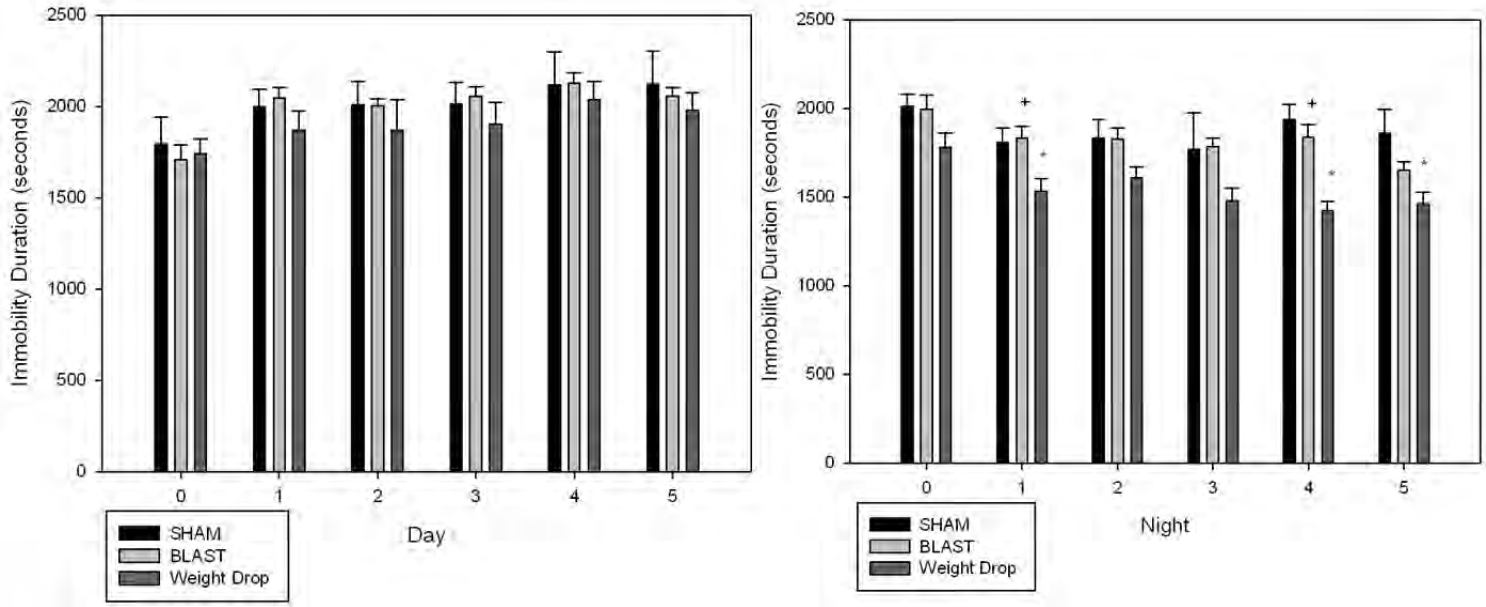

Figure 19: Immobility duration during the day (light cycle) and night (dark cycle).

The animals were placed in the Laboras bioactivity chambers for day -5 to day 0 pre mTBI and days 0-6 post mTBI. The Laboras software tracks behaviors such as grooming, locomotion, immobility, and climbing using a cage vibration platform system.

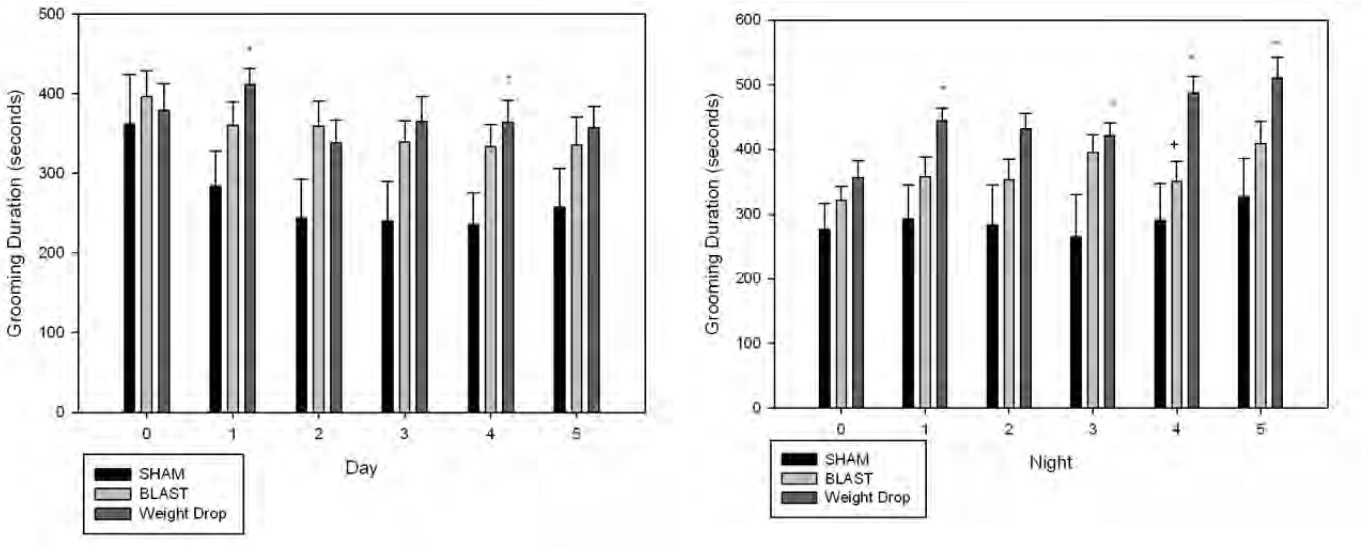

Figure 20: Grooming duration during the day (light cycle) and night (dark cycle)

The animals were placed in the Laboras bioactivity chambers for day -5 to day 0 pre mTBI and days 0-6 post mTBI. The Laboras software tracks behaviors such as grooming, locomotion, immobility, and climbing using a cage vibration platform system. The weight drop animals showed significant overgrooming as compared to sham animals (indicated by *) on four out of the six nights spent in the chambers as well as two of the six days. The blast group showed significant overgrooming as compared to shams (indicated by +) only on night four.

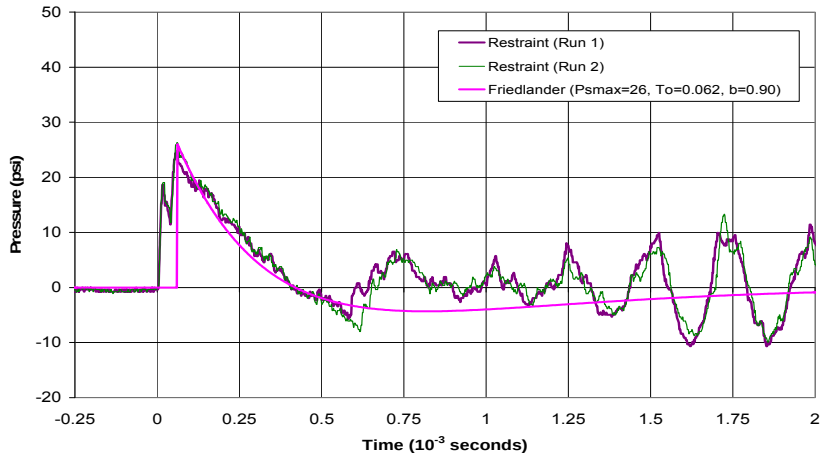

Figure 21: Independent replications (run 1 and 2) induced nearly identical blast waveforms. These blast waves rapidly reach a peak overpressure (26 psi) and are followed by a rapid underpressure which closely fits a Friedlander function (pink line).

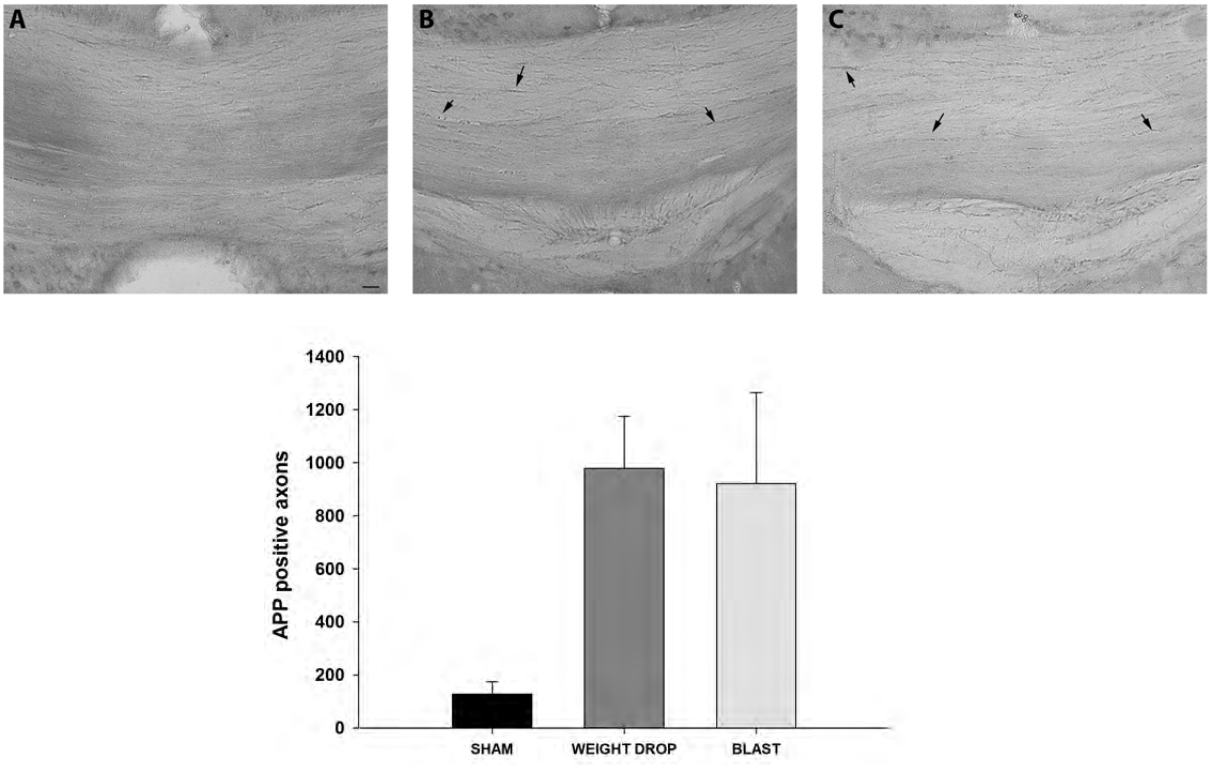

Figure 22: Evaluation of accumulation of amyloid precursor protein (APP) in axonal tracts after mTBI from sham group (panel A), weight drop group (panel B), and blast-induced brain injury group (panel c). The lower panel is a stereological quantification of the number of APP positive axons detected in the corpus collosum.

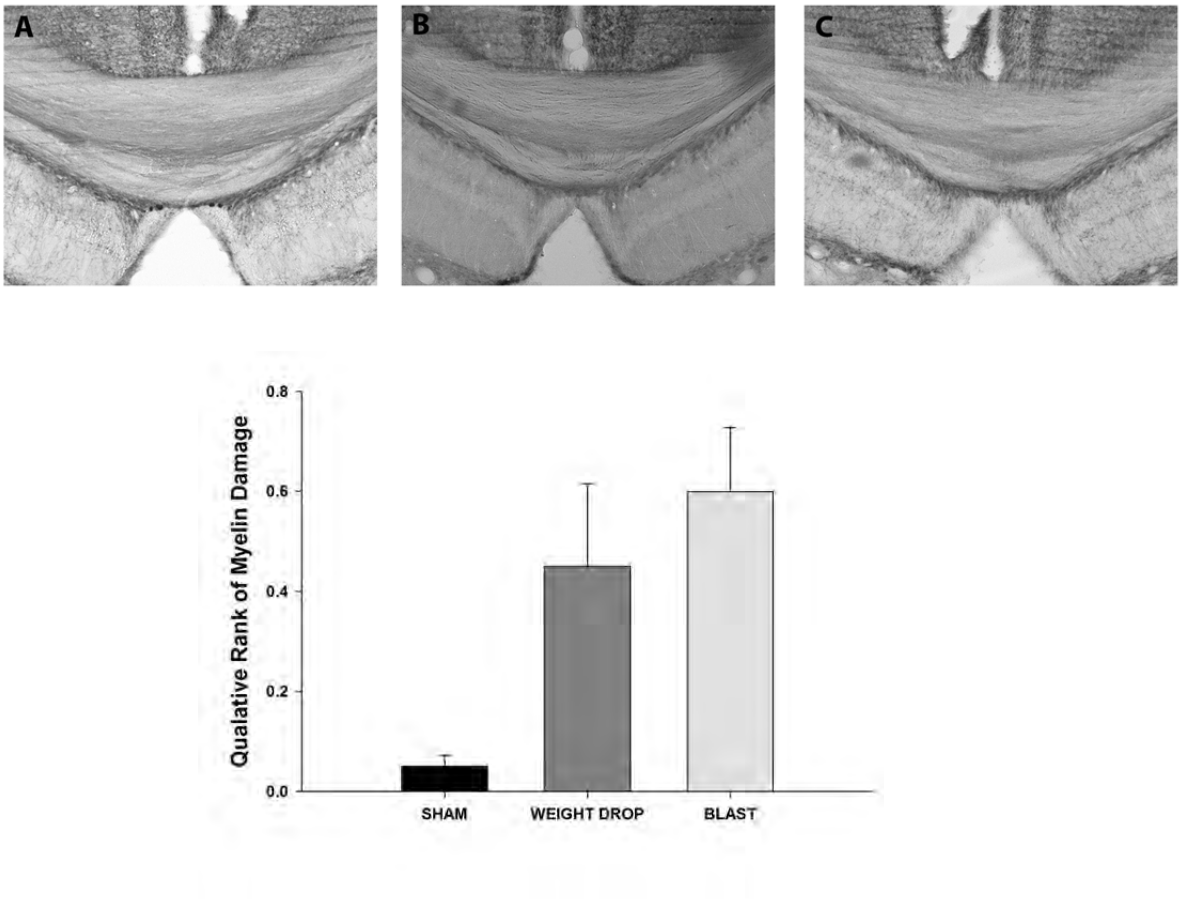

Figure 23: Evaluation of myelin integrity using immunohistochemistry against myelin basic protein. Representative micrographs from mice in the sham group (panel a), weight drop group (panel b) and blast-induced mTBI group (panel c) are shown. Ranking of myelin damage was conducted by an investigator naïve to the treatment groups using the following system: 0=no damaged myelin; 1= some damaged myelin; and 2= extensive damaged myelin. As shown by the rankings, on average some damaged myelin was observed after weight drop or blast-induced mTBI.